THE PENNSYLVANIA STATE UNIVERSITY
SCHREYER HONORS COLLEGE

DEPARTMENT OF ENGINEERING SCIENCE AND MECHANICS

EFFECTS OF VARIABLE AMPLITUDE LASER SCANNING FOR WIRE-FED METALS ADDITIVE MANUFACTURING

CHRISTOPHER H. WALSH
SPRING 2020

A thesis
submitted in partial fulfillment
of the requirements
for a baccalaureate degree
in Engineering Science
with honors in Engineering Science

Reviewed and approved* by the following:

Abdalla R. Nassar
Associate Research Professor
Thesis Supervisor

Lucas J. Passmore
Associate Teaching Professor of Engineering Science and Mechanics
Honors Advisor

Judith A. Todd
Department Head
P. B. Breneman Chair and Professor of Engineering Science and Mechanics

*Signatures are on file in the Schreyer Honors College and Department of Engineering Science and Mechanics.

Abstract

Metals additive manufacturing (AM) utilizing scanning laser optics is currently an under-explored topic, but has potential to offer greater process control and performance. One of the greatest drawbacks of AM is long processing times due to low deposition rates. However, optical systems that enable the rapid scanning of a high-power beam allow for more material to be deposited per unit of time. The introduction of a non-linear beam path creates more complex engineering problems to solve, but it also introduces more variables that can manipulated for greater control over the printing process. One such variable is the pattern of the scan path itself. By dynamically manipulating the scanning path of the beam, the imparted energy distribution to the substrate can be tailored however the process controller wants. For example, a pattern of linearly attenuating scan amplitude can configure material overlap when two beads meet at an angle. The calculated input energy, among other factors, can also be used to estimate the bead geometry. In order to predict the resulting imparted energy distribution, a series of software has been developed to characterize a high-power laser beam, generate a scanning pattered based on sliced CAD data, and iteratively simulate the energy imparted on the substrate using the properties of the characterized beam. Studied here is a hot wire-fed directed energy deposition (DED) AM system utilizing an ABB Robotics industrial arm with 6 degrees of freedom, an IPG Photonics continuous wave 12kW ytterbium fiber laser, and a Laser Mechanisms FiberScan™HR laser scanning system.

Table of Contents

List of Figures

List of Tables

List of Symbols

d_σ	Beam diameter, p. 20
$d_{\sigma 0}$	Beam waist diameter, p. 19
$d_{\sigma x}$	Beam diameter in the x axial direction, p. 19
$d_{\sigma y}$	Beam diameter in the y axial direction, p. 19
I	Intensity distribution of a laser beam, pp. 17, 18
λ	Wavelength of beam, p. 20
M^2	Beam quality factor, pp. 19, 20
ω	Beam radius, p. 20
ω_0	Beam waist radius, p. 20
P	Total power of a laser beam, p. 17
ϕ	Azimuth angle, p. 20
R	Radial distance from the center of a Gaussian beam, p. 17
r	$\frac{1}{e^2}$ radius of a Gaussian beam, p. 17
σ_x^2	Second order moment in the x axial direction, p. 18
σ_y^2	Second order moment in the y axial direction, p. 18
Θ	Divergence angle, p. 21
θ	Divergence half angle, p. 16
$\bar{X}$	First order moment in the x axial direction, p. 18
$\bar{Y}$	First order moment in the y axial direction, p. 18

z_0 Location of the beam waist along the axis parallel to the propagation direction of the laser beam, p. 19

Z_R Rayleigh range, pp. 19, 22

Acknowledgments

I would not have been able to complete this thesis without the plentiful help from the following persons and organizations.

The Center for Innovative Materials Processing 3D (CIMP-3D) and the Applied Research Laboratory at Penn State (ARL Penn State) for providing the equipment and funding needed.

Abdalla R. Nassar for teaching me much of what I know about laser optics, guiding my progress, and providing feedback throughout the development process.

Wesley F. Mitchell for providing me with direction, explaining the functionality of the AM systems used in the investigation, and helping to operate the Primes Focus Monitor system along with Evan J. West.

Edward W. Reutzel for project guidance and funding acquisition.

Trevor J. Haas for gathering data from motor controllers and communicating the point, velocity time (PVT) control input syntax.

My greatest gratitude is extended to each of you.

This material is based upon work supported by the United States Navy under Contract No. N00014-19-C-2034. Any opinions, findings and conclusions or recommendations expressed in this material are those of the author(s) and do not necessarily reflect the views of the United States Navy.

Chapter 1 Introduction

1.1 Problem Statement

Additive manufacturing (AM) has had a large impact on the manufacturing industry. AM roots are found in the use of photopolymers, or plastics that harden when exposed to certain types of light, in 1981 [1, 2]. However, these plastic creations did not yet have the mechanical properties to be of use in an industrial setter and thus were mostly used for rapid-prototyping, a practice still common today. industrial AM was once used almost solely for prototyping or purely cosmetic builds, now functional parts can be created out of polymers, metals, and ceramics. Advances in metals additive manufacturing are of particular interest to industry [3] because of the plethora of advantages over traditional manufacturing methods as well as unique applications. This includes, but is not limited to:

- a reduction in production lead-times as well a lower cost for replacement parts,
- the ability to repair sensitive parts with minimal distortion,
- a drop total part counts for assemblies due to part consolidation, and
- the ability to manufacture parts on-demand rather than in bulk.

The method of AM most relevant to the work in this thesis is Directed Energy Deposition (DED) with a laser as the energy source. DED can be performed with either a metal powder [4] or with a wire feedstock [4, 5]. In the case of powder, a laser is directed towards the work piece, also called the substrate, creating a small collection of molten metal called the melt pool [6]. Fine grain metal powder is ejected from a feeding system along a path that leads through the laser beam and into the melt pool [4]. The now

molten powder adds its mass to the melt pool and the process continues. While this is occurring, either the printhead or the substrate moves along a path specified by a path planning algorithm according to the desired part geometry. This process is repeated layer after layer until the entire part is complete [7].

The process is similar in the case of a wire feedstock. The laser is still directed towards the substrate to create a melt pool, but in this case a wire is fed directly into the melt pool to add to its mass. In hot wire-fed DED, an electric potential is applied to the wire and substrate. When contact is made between the two metals an electric current is able to flow which heats the metal wire significantly before it is heated to the melting point by the laser. The preheating of the wire reduces the amount of energy that the laser must impart to melt the metal. This stabilizes the melting process and increases the maximum deposition rate of the system [8]. This additional thermal input from the electrical current is advantageous because lasers are only able to transform a certain percentage of their input power into usable optical power [9]. The ratio of input power to output power is called wall-plug efficiency. Wall-plug efficiency is often in the range of 25%-30%, but today there are lasers that can get above 60%, although sometimes such laser are not particularly useful due to poor beam quality [10]. The laser used in the investigations presented in this thesis has a wall-plug efficiency of 25%-27.3% [11]. Furthermore, a significant portion of the laser's energy is not absorbed by the material and is instead reflected [12]. Generally only 5%-50% of the energy is absorbed.

Wire-fed DED systems are less restricted in size than their powder-fed counterparts because wire feedstock is both cheaper and safer to work with then metal powder [13]. Metal powder has much more surface area than metal wire which rapidly increases the rate of oxidation. As the metal oxidizes, it produces heats, which expedites the oxidation process. This chemical reaction feedback loop makes metal powder susceptible to spontaneous combustion. [14]. This is because a complex powder feeding system with air pumps and tubing is not needed, but is instead replaced by a comparatively simple wire-feeding system. This simplicity opens up the design space for added mobility of the printhead. The experiments performed in this investigation are performed on a wire-fed DED system that makes use of an industrial-sized ABB robotic arm with a printhead at the end of it. The system allows printing over a 2m x 3m x 3.5m area with six axes of freedom. The capability to produce parts that are much larger than those standard metals AM system can opens design space the increases the applicability of AM.

One of the largest issues faced by AM systems is how long it takes to complete printing a part [13]. Build time can be reduced by a variety of methods each with

their own advantage and disadvantages. One of the simplest solutions is increasing the translational speed of the printhead. However, as the heat source moves more rapidly, the energy density distributed on the substrate is decreased along with the heat effected zone [15]. Problems such as lack of fusion are likely to occur in situations such as these [16]. This issue can be mitigated by increasing the output power of the laser, but this is restricted by the capabilities of the laser model being used. Another method is choosing a build orientation that is more efficient [17]. Some geometries require extensive support structures in order to build in certain orientations, but almost no support is needed in others. By optimizing orientation, operators can not only reduce build time, but also save material. A more recently developed approach involves using a scanning laser optics system in order to widen the heat effected zone [18]. This thesis focuses on expanding the capabilities of this approach.

1.2 Design Needs

1.2.1 Equipment and Software

The equipment to be used in the investigation includes the following:

- PRIMES Focus Monitor to take measurements of the laser;
- ABB robotic arm system to move the printhead in a controlled manner;
- IPG Photonics YLR-12000-C Continuous Wave Ytterbium Fiber Laser as a heat source;
- FiberScan™ HR to control the planar motion of the laser

1.2.2 Ethics and Safety

1.2.2.1 Ethics

All engineers are bound to a collection of ethics to guide their behavior. Depending on the nature of their work, any malpractice could lead to the harm of those who interact with it. As lasers are being used in this investigation it is of utmost importance that the dangers of working with high-powered laser is stressed to avoid any injuries in the case of another team attempting to confirm the results discussed in this document. Furthermore, additive manufacturing comes with its own risks. Molten metal can be ejected from the

melt pool due to forces caused by vaporization. This material can cause damage to either flesh or sensitive equipment. Therefore it is best practice to either have the printing environment contained or keep a safe distance.

1.2.2.2 Pubic Health and Safety

Whenever working with high-power lasers, safety must be kept as a priority. Even low wattage lasers can cause temporary or permanent eye damage including loss of vision [19]. This ever-present risk requires that measures are taken to make sure all staff working with the laser are safe. The system used in the experiments for this investigation is in an enclosed room with only one window. The window is equipped with a protective coating that prevents the danger light from passing through. It is forbidden to activate the laser while someone is in the processing room or while the door to the processing room is open. A specialized set of cameras and other sensors are used to safely monitor the workpiece when an experiment is running. These sensors, as well as the printing head housing, are covered by heat shields to protect them from reflected and radiated energy.

1.2.3 Environmental and Economic Considerations

Due to lasers' inherent inefficient use of power [10,12], great care should be taken minimize the amount of time the laser is in use. Experiments should be fully planned in advance and executed efficiently.

Additive methods, compared to subtractive manufacturing methods, use less material to yield parts of equal mass. This is because only the material that is needed to build the part and support it during production is used rather than starting with a block of material and removing unwanted volume as waste. By reducing the production of waste material, the necessity to produce metals that are environmentally and economically taxing to mine and refine is also reduced.

The ability to produce part on a "as needed" basis is yet another benefit of AM. Instead of having to mass produce parts during a production line, such as is currently done in the automotive industry, instead replacement parts can be printed as the need arises. Thus waste is reduced and money is saved.

1.2.4 Cultural Impact

The desires and needs of the world are constantly changing, and so too should the products they use. AM provides industries with the ability to quickly develop, produce,

sell modular changes and upgrades to their products; similar to how software is constantly being improved and updated.

1.3 Objectives of the Thesis

The purpose of the investigation in this thesis is to gain a better understanding of the possibilities of dynamic scanning patterns for metals additive manufacturing. While investigating the current literature, it was found that this topic is very lightly explored. The relevant research is discussed in Cp. 2. The most similar research was by *Pekkarinen et al.*. Their team's focus was on manipulating the deposition bead's cross-sectional geometry by means of dynamically adjusting laser power throughout the scanning pattern [18, 20].

It is predicted that by manipulating the scanning path the density of the energy imparted on the substrate can be controlled to get desired cross-sectional geometry. Since dynamic scan path adjustment is a very large topic and has barely been explored, this thesis seeks to investigate a simplified subset of the possibilities. The subset chosen is the amplitude of the scan path. The experiments entail a single beam deposition with a linearly reduced amplitude.

One possible application of a reduced amplitude scan path is filling in tight spaces on a build. For example, when two scan paths intersect at an angle, a "stair step" [21] effect is encountered. Please see Sec. 8.2 for more information about the "stair step" effect. With traditional AM methods, this space would have to be filled by depositing a bead of a width that is too great. This excess of material often leads to issues on the next layer that could continue to compound through to even more layers. By dynamically adjusting the width of the bead, the region could be filled with a proper amount of material. Fig. 1.1 offers a visual representation of this concept.

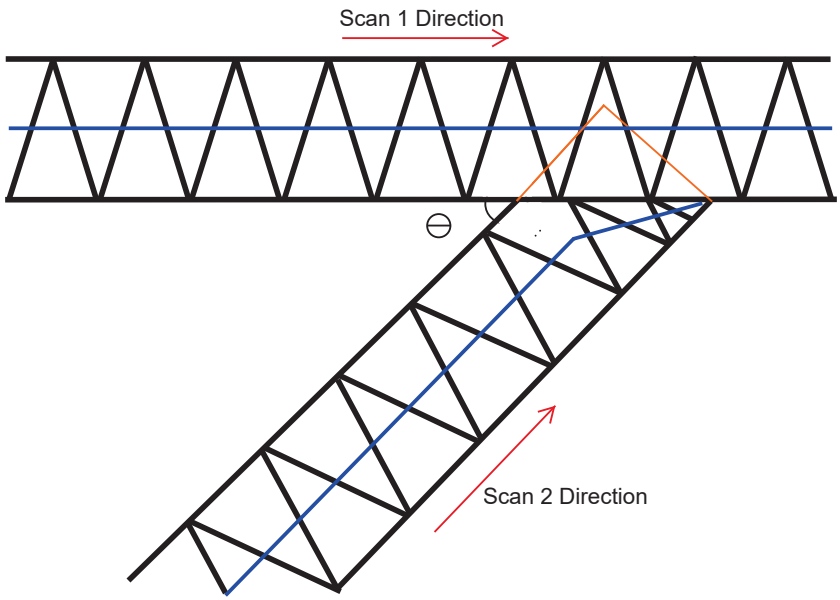

Figure 1.1. When two scan beads intersect at an angle Θ, a region of overlap is created, drawn in orange. This excess of material can lead to issues on subsequent layers. In order to avoid this issue, the width of the bead can be adjusted by reducing the amplitude of the scan pattern of Scan 2. The translational direction of the printhead, shown in blue, is adjusted to remain in the center of the scan pattern to avoid uneven feeding of material.

Chapter 2
Literature Review

2.1 Scanned Laser Optics for Additive Manufacturing

Scanning laser optics have been used for laser cladding[†] for over 40 years since Belmont and Castagna published their paper covering the topic in 1979 [23]. In the last decade, there has been somewhat of a resurgence in the interest of using scanning laser optics for metals additive manufacturing. Two groups have published the majority of the recent papers. The first, Klocke *et al* [8, 22] investigated using scanning optics with wire-fed DED. The second, Pekkarinen *et al* [18,20,24–26], investigated with the use of powder-fed DED.

Using a scanned laser path provides a plethora of benefits. By spreading out the energy imparted by the laser over a larger area on the substrate it is possible to use a higher power laser without inducing excessive vaporization [18]. A higher power laser enables a higher feedstock input rate while still fully melting all material [24]. This directly translates to a higher deposition rate. Higher deposition rates make larger builds more economical by reducing long build times. Furthermore, by introducing extra processing parameters pertaining to the scan pattern, greater flexibility and control over the printing process is gained [8, 20]. The most useful process parameters are as follows:

- scan amplitude,
- scan frequency,
- scan pattern,

[†]Laser cladding is a form of surface treatment that uses a laser to deposit a layer of new material atop a pre-existing part. Cladding avoids putting excessive heat into the substrate, therefore avoiding excessive dilution and warping [22].

- laser power,
- laser spot size,
- material feed rate, and
- printhead velocity.

Each has a measurable impact on the printing process and/or the resulting bead geometry [8, 24]. The following sections discuss the effects.

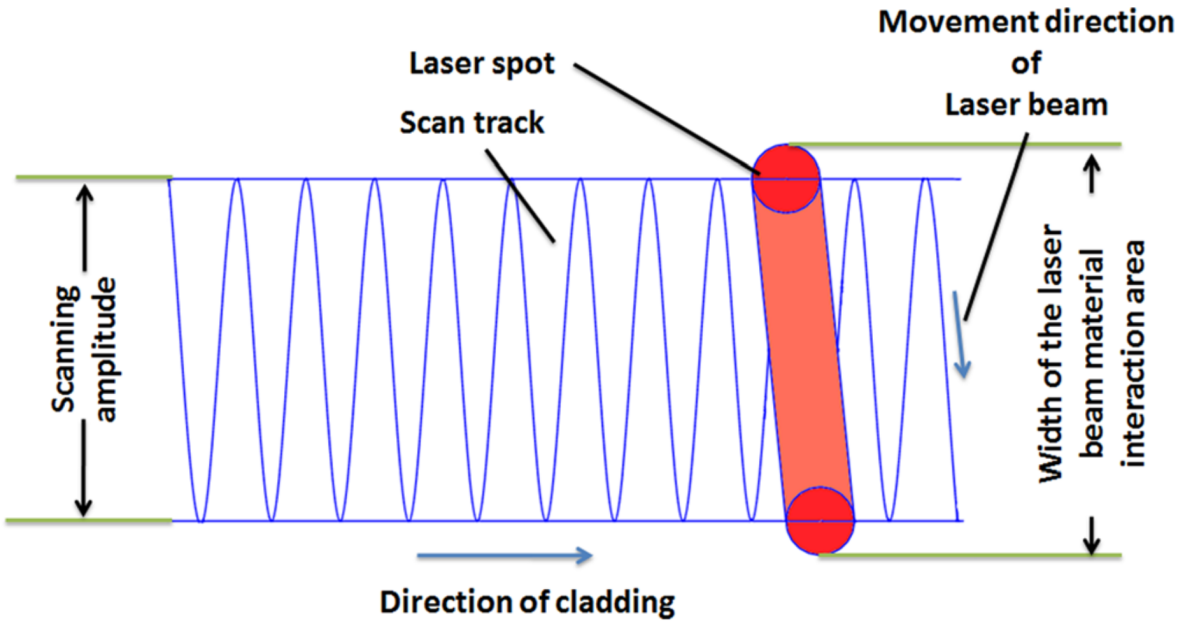

Figure 2.1. An example of a scanned beam path using a sine wave. The direction of cladding is the direction of the translational velocity of the printhead. Notice that the size of the laser beam causes the width of the interaction area to be the scan amplitude plus the diameter of the beam. Image from *Pekkarinen et al.* [18]

2.1.1 Effects of Process Parameters

Adjustment to any given processing parameter is not a guarantee of a better deposition. In most cases, benefits are gained at the cost of causing worse results in another aspect of the printing process [18, 20, 24–26]. Finding an optimal balance to gain the best results for a given situation can be difficult.

2.1.1.1 Scan Amplitude

When working with high-power lasers as heat inputs it is nearly impossible to completely avoid vaporization, but scanning the laser beam provides additional techniques to reduce it [8, 18, 24, 25]. Vaporization is undesirable because it adds a degree of uncertainty to the process. The plume of vaporized metal particles can act to defocus the beam as well as attenuate the energy, changing the energy distribution imparted on the substrate [27]. In the case of high-power lasers, the plume of vapor can even detach from the substrate and travel towards the laser source [28]. A plasma exhibiting this behavior is often referred to as a laser-supported combustion wave. A larger scan amplitude increases the area over which the laser energy is distributed, reducing local energy density and producing a wider bead [25]. Lower local energy density reduces the risk of excessive material vaporization [18]. However, spreading out the input energy too much can lead to lack of fusion due to either the substrate or feedstock not melting fully [18].

Additionally, *Pekkarinen et al* discovered that a larger amplitude caused significant "waves" in the melt pool and the bead [26]. In the article, this phenomenon is explained as a consequence of vaporization. As vapor rapidly expands out from the melt pool it creates an area of high pressure. This vapor pressure causes changes in the flow of the melt pool as well as the environment nearby the melt pool and can even eject molten material out of the melt pool on unto the surrounding area [29]. In the case of power-fed DED, induced flows in the inert gas environment can even prevent new powder from entering the melt pool [18].

A small scan amplitude can lead to excessive vaporization because the energy is not sufficiently spread out. However, *Pekkarinen et al* concluded that a smaller amplitude lead to a less "wavy" bead because the melt pool did not have the time to swing back and forth, and instead "pulsed" [26]. "Pulsing" resulted in a bead that was smoother and taller than its large amplitude counterpart.

2.1.1.2 Scan Frequency

Scan frequency has a similar effect to scan amplitude on local energy density [18]. Frequency is inversely related to local energy density so in general a higher frequency is more likely to lead to a stable build process. 40Hz was found to be somewhat of threshold between stable and unstable builds with the system used by *Pekkarinen et al* [24]. Furthermore, a higher frequency yielded a more homogeneous energy distribution on the substrate [8]. Non-homogeneous energy distributions can either be of great benefit

or reduce the quality of the build. These effects will be discussed in detail in Sec. 2.1.1.4.

Pekkarinen et al found low frequencies could lead to high local energy intensity at the extremities of scanning amplitude due to dwelling. In the case of a the sinusoidal scan pattern used by Pekkarinen's team's system, the laser spot spends additional time at the peaks of the amplitude. It was reported that dwelling caused keyholing*

There are, however, limitations to scan frequency imposed by laws of physics. Infinite acceleration is impossible and so galvanometers that control the mirrors used to scan the laser can only reach a maximum frequency. The largest frequency used in the literature was 150Hz [20].

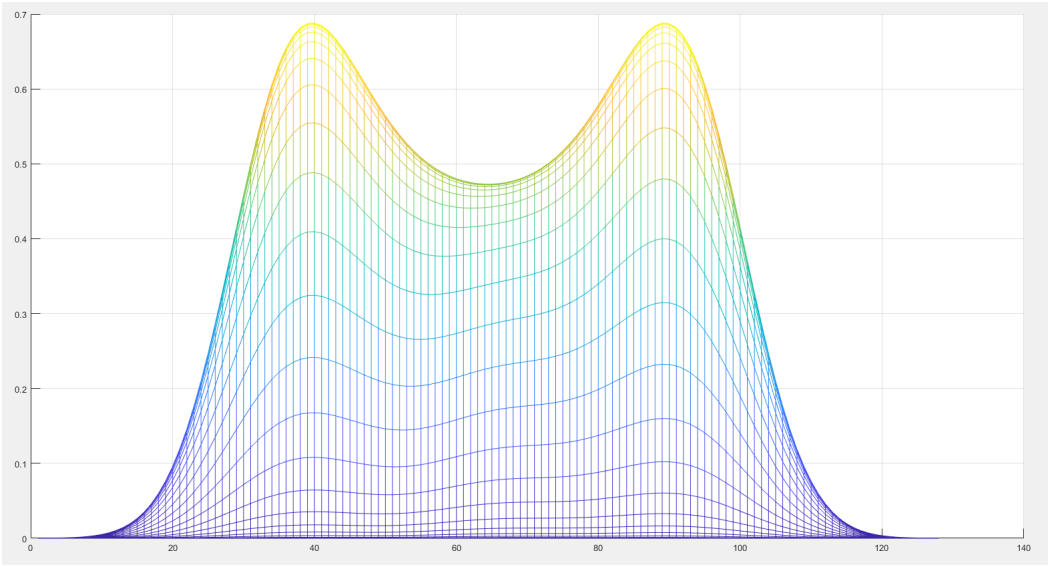

Figure 2.2. The profile of an energy distribution simulation generated using a sinusoidal waveform. The two-peaked distribution is called "viper teeth". The axial values in this example do not relate to a physical experiment, this image is purely intended to show the shape.

2.1.1.3 Scanning Pattern

Scanning patterns can vary from sinusoidal, triangular, circular, elliptic, or any arbitrary waveform. In the literature, *Klocke et al* reported using a circular pattern [8, 22] while *Pekkarinen et al* reported a sinusoidal pattern [18, 20]. The pattern used has a great effect on how energy is distributed on the substrate. As discussed in Sec. 2.1.1.2, high local energy intensity causes vaporization, and in extreme cases, can push the printing

*Keyholing is a phenomenon that is caused when the laser is able to vaporize a significant amount of material, including the substrate. A hole is created by the vapor pressure which can collapse, trapping air or impurities once the material cools. Keyholing, while it has niche uses, should generally be avoided.

process into a keyholing regime. The non-homogeneous energy distribution caused by a sinusoidal scanning pattern has been discussed in the literature at length and has its own name, "viper teeth". "Viper teeth" distributions are undesirable because of the high local energy density at the extremities of the scan pattern caused by laser dwell time. See Fig. 2.2 for an example of what this distribution looks like.

2.1.1.4 Laser Power

To avoid the shortcomings of a scanning pattern it is necessary to adjust other parameters to compensate for the non-homogeneous energy distribution. One such method of compensation is dynamically adjusting laser power in regions of dwell time. In their investigations, *Pekkarinen et al* were able to create beads with preferable cross-sectional geometry despite utilizing a sinusoidal scan pattern by adjusting laser power levels at 32 points within each period of the wave [20]. The best results were achieved when power was diminished near the peaks of the sine wave. Doing so compensated for the energy density peaks characteristic of "viper teeth" distribution. Additionally, the team was able to create unique cross-sectional geometry such as a "canal" by increasing power on the extremities of the amplitude while decreasing power near the center of the sine wave. The "canal" is formed by two separate beads separated by a region of no deposition between them. This study proved that it is possible to alter bead geometry by changing the energy distribution imparted on the substrate. The investigation for this thesis seeks to exploit this relation between energy distribution and bead geometry in order to dynamically adjust the bead's width as a function of the translational location.

2.1.1.5 Laser Spot Size

When discussing laser power, it is necessary to also consider laser spot size. Spot size describes the diameter of the beam at the location it interacts with the substrate. Defining the diameter of a laser beam is a involved process and is discussed at length in Sec. 2.2. The area over which the beam is interacting with material has a large impact on the power distribution. As the spot size of the laser increases, the average power per unit area is reduced [18].

ARL Penn State has found that when working with high-powered lasers it is often advantageous, if not necessary, to operate using a region of the laser that is not at full focus. This is because vaporization is almost unavoidable when working at focus as the extent of the laser power is distributed over a small area of the substrate. Expanding the spot size by working with a region of the laser away from its focus location allows the

same laser power to be used without causing vaporization. As discussed previously, using a higher power allows more feedstock to be melted per unit time, increasing deposition rate.

2.1.1.6 Material Feed Rate

The rate at which material is introduced into the melt pool affects both the deposition rate as well as the ability of the heat source to melt all the material added. As discussed earlier, one of the greatest benefits of using scanned laser optics is that higher deposition rates can be achieved [8]. Adding more material per unit time requires more energy to fully melt all the input material hence why high-powered lasers are utilized for such processes.

Operators must be conscious of not only how extra feed material will affect the melt pool temperature, but also its effect on the geometry of the resulting bead once it cools and solidifies [24]. *Pekkarinen et al* stated that increasing feed rate with all other processing parameters held constant would result in a taller bead while not significantly effecting width [24].

Furthermore, an increase in the amount of material requires more energy to fully melt the material. Adding more material than the heat source can melt puts the process at an increased risk of lack of fusion.

2.1.1.7 Velocity

The effect of translational velocity of the printhead is multifaceted. By moving the printhead more rapidly, the total print time can be reduced. However, this benefit does not come without a cost. A greater velocity reduces the amount of feedstock per unit area, if the feed rate is held constant. With less material in a given area, the resulting bead will have a reduced cross-sectional area. If beads are smaller, more of them are required to build the part. A higher translational speed can also lead to increased levels of dilution between the substrate material and the feedstock material [24, 30, 31]. This dilution is caused by the laser being able to directly interact with the substrate material instead of the melt pool. At lower translational velocities, the melt pool is able to flow forwards, ahead of the laser spot, and cover the substrate material, shielding it from direct laser light. If the laser spot moves faster than the front of the melt pool, the substrate will be melted more than necessary for a strong bond and lead to greater degrees of dilution. Some dilution is necessary for a strong bond to the substrate, but too much dilution can change the material properties.

Furthermore, the velocity of the printhead can affect the geometry of the bead. As the velocity increases, both the height and the width of the bead will be reduced [24]. However, this can be compensated for by increasing the material feed rate assuming an adequate increase in energy input is included as well.

2.2 Laser Beam Characterization

As mentioned in section 2.1.1, the local energy density imparted by the laser has a large effect on the resulting bead and the printing process. It is therefore of great benefit to be able to predict if the imparted energy density will be too great, pushing the process into a keyholing mode, too little, pushing the process into a lack-of-fusion mode, or just right, resulting in the desirable conduction mode. An iterative computational simulation was developed during this investigation for this purpose. To make an effective simulation, the laser system being simulated must be fully measured.

Beam characterization is the process of finding numerical values that describe all aspects of a laser beam. It is of utmost importance to have a full knowledge of the beams being used in order to design the optical systems that control them properly as well as understanding the laser-material interactions that arise. Therefore standards were devised to help scientists and engineers to effectively communicate the properties, or characteristics, of the laser beams they use. The ISO standard* is most widely used and the methods it describes are used in the software used in this investigation.

An in-detail discussion of how the software calculates the beam characteristics can be found in Chapter 3.

*ISO 11146 [32] series of standards dictates how to characterize stigmatic and astigmatic beams as well as how to account for noise in the data

Chapter 3
Methodology

This section will discuss, in detail, the three pieces of software developed and used in this investigation beginning with the beam characterization software, then moving to the laser path planning algorithm, and ending on the scripts that approximate energy density imparted on the substrate as well as power density distributions.

3.1 Beam Characterization Software

Lasers are used all around the world every day. They perform a variety of tasks from indicating a location for students to look on a presentation, to transferring data, to processing materials. In the latter two applications, it is incredibly important to have a full knowledge of the beams being used in order to design the optical systems that control them as well as understanding the laser-material interactions that arise.

Beam characterization is the process of finding numerical values that describe all aspects of a laser beam. These properties describe the shape of the beam as it propagates through space, the cross-sectional power density distribution at a given plane, the region of the beam suitable for operational proposes, and much more. With a more complete understanding of a beam's properties comes the knowledge of how to leverage it for whichever purpose it is intended to perform.

The beam characterization software developed in this work is able to take data on the laser's cross-sectional power density distribution (see section 3.1.1), calculate the defining beam characteristics, and plot the relevant data.

Laser beams are used extensively in AM from powder bed fusion (PBF) to directed energy deposition (DED) [12]. Lasers are a great method of delivering a large amount of energy to a small area which makes them one of the premier options for sintering or melting material. In order to produce the highest quality parts possible, every aspect

of the AM system must be understood and documented. The optical system is no exception to this rule. Standards were devised to enable scientists and engineers to effectively communicate the properties, or characteristics, of the laser beams they use. The ISO standard* is most widely used and methods it describes are employed in the beam characterization software.

3.1.1 ISO Standard

The first step in analyzing a beam is to take measurements of the cross-sectional power density distribution at a number of locations along the propagation direction of the beam. The cross-sectional power density distribution is the measure of the power applied by the beam over an area. According to the ISO standard, at least ten cross-sectional measurements must be taken with roughly half of them falling within one Rayleigh length (see Sec. 3.1.1.6 in either direction from the beam's waist (see Sec. 3.1.1.1 and the other half distributed beyond two Rayleigh lengths [32]. The thinnest cross-section of the beam, also called the beam waist, must be included within the bounds of the measurement in order to get the most accurate result possible.

There are a number of properties that can be calculated by analyzing the cross sectional data. Some of the most important properties are:

- waist diameter,
- beam quality factor (M^2),
- azimuth angle,
- divergence angle,
- beam parameter product (BPP), and
- Rayleigh range.

The following sections will go over the mathematics used to calculated each of these properties.

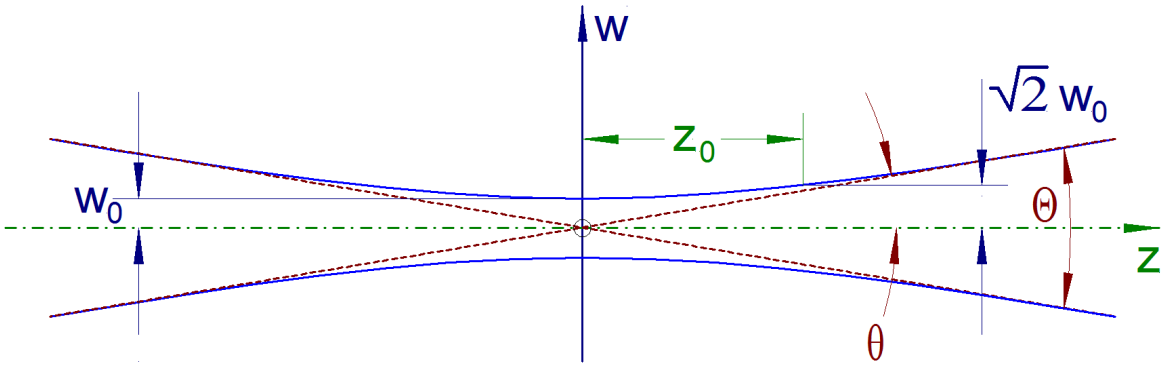

Figure 3.1. Visual representation of the waist W_0, Rayleigh range Z_0, half angle divergence θ, and full angle divergence Θ. The figure is not to scale. Image created by Bautsch [33].

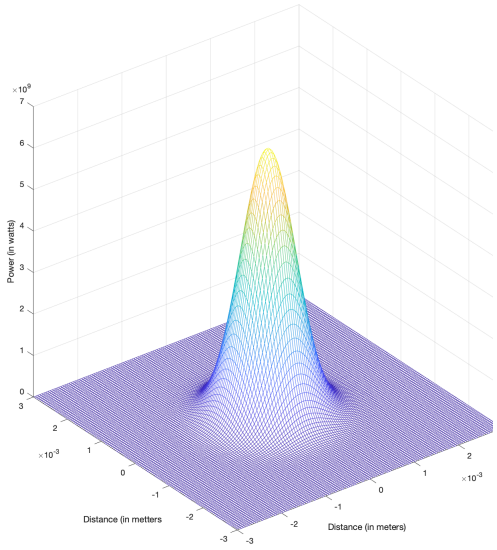

Figure 3.2. An example of an isometric view of the cross-sectional power density distribution of a 10kW Gaussian beam with a radius of 1mm. An angled view reveals the radial symmetry of the power density distribution.

3.1.1.1 Waist Diameter

The term "radius" or "diameter" when referring to a laser beam can be misleading since beams do not have a distinct edge*. To illustrate this point, observe the Gaussian beam's

*ISO 11146 [32] series of standards dictates how to characterize stigmatic and astigmatic beams as well as how to account for noise in the data

*Aside from idealized top hat beams which have a region of constant power and outside of that region power is zero.

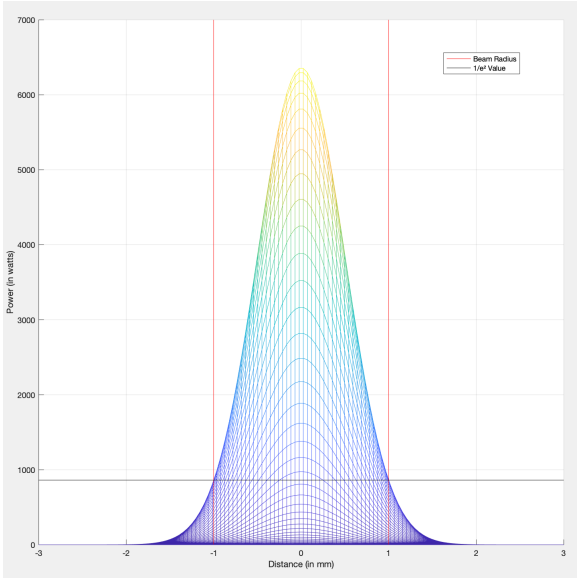

Figure 3.3. An example of a side view of the cross-sectional power density distribution of a 10kW Gaussian beam with a radius of 1mm. A side view reveals the familiar 2-dimensional Gaussian Curve. The radius of the beam is marked in red, notice that the power is not zero at that location, but rather it is $\frac{1}{e^2}$ of the maximum power.

power density distribution presented in Fig. 3.2. A Gaussian beam is an idealized laser beam whose intensity follows that of a three-dimensional Gaussian distribution. The governing equation for the cross-sectional power density distribution of a Gaussian beam is given below:

$$I(x,y) = \frac{2P}{\pi r^2} \exp\left(-2\left(\frac{R}{r}\right)^2\right) \tag{3.1}$$

$$R = \sqrt{x^2 + y^2}$$

where I(x,y) is the cross-sectional power density distribution, P is the power of the beam, and r is the radius of the beam. A visual example of a Gaussian distribution can be seen in Fig. 3.2 and Fig. 3.3. By definition, a Gaussian curve approaches 0 at $\pm\infty$, therefore the power is not 0 watts past the radius used as an input in Eq. 3.1. The radius used is not what one may consider a "traditional" radius, but rather it is called the "$1/e^2$" radius because it makes the radial distance at which the beam's power is $1/e^{2*}$ of its value at the origin.

There are multiple methods used to calculate the 'diameter' of the distribution. Some

*This equates to approximately 0.13533528323

of the most popular are the Second Moment (also called $D4\sigma$), D86, and knife-edge methods. The method used by the ISO standard as well as the Laser beam characterization software is the Second Moment method [32].

The Second Moment method defines the diameter as the width of four standard deviations of the power density distribution [32]. First the data is centered by calculating the first order moment using Eqs. 3.2. Where $I(x, y, z)$ is the function describing the power density distribution of the beam at a particular plane distance z from some reference point. The resulting first order moment is notated with a bar over the letter of the axis it is taken about.

$$\begin{aligned} \bar{X}(z) &= \frac{\int_{-\infty}^{\infty}\int_{-\infty}^{\infty} I(x,y,z)x\,dx\,dy}{\int_{-\infty}^{\infty}\int_{-\infty}^{\infty} I(x,y,z)\,dx\,dy} \\ \bar{Y}(z) &= \frac{\int_{-\infty}^{\infty}\int_{-\infty}^{\infty} I(x,y,z)y\,dx\,dy}{\int_{-\infty}^{\infty}\int_{-\infty}^{\infty} I(x,y,z)\,dx\,dy} \end{aligned} \tag{3.2}$$

The first order moments are used to normalize the data for calculating the second order moments.* By recentering each plane, any bias caused in the calculation of the second order moment is avoided.

$$\begin{aligned} {\sigma_x}^2(z) &= \frac{\int_{-\infty}^{\infty}\int_{-\infty}^{\infty} I(x,y,z)(x-\bar{X})^2\,dx\,dy}{\int_{-\infty}^{\infty}\int_{-\infty}^{\infty} I(x,y,z)\,dx\,dy} \\ {\sigma_y}^2(z) &= \frac{\int_{-\infty}^{\infty}\int_{-\infty}^{\infty} I(x,y,z)(y-\bar{Y})^2\,dx\,dy}{\int_{-\infty}^{\infty}\int_{-\infty}^{\infty} I(x,y,z)\,dx\,dy} \\ {\sigma_{xy}}^2(z) &= \frac{\int_{-\infty}^{\infty}\int_{-\infty}^{\infty} I(x,y,z)(x-\bar{X})(y-\bar{Y})\,dx\,dy}{\int_{-\infty}^{\infty}\int_{-\infty}^{\infty} I(x,y,z)\,dx\,dy} \end{aligned} \tag{3.3}$$

The second moments can then be used to calculate the beam diameter, where $d_{\sigma x}(z)$ and $d_{\sigma y}(z)$ are the diameters of the beam along the x and y axis at some distance (z) along the

*The σ values are not actually squared. The exponent is purely notational [32].

propagation direction.

$$d_{\sigma x}(z) = 2\sqrt{2}\left\{\left({\sigma_x}^2 + {\sigma_y}^2\right) + \gamma\left[\left({\sigma_x}^2 - {\sigma_y}^2\right)^2 + 4\left({\sigma_{xy}}^2\right)^2\right]^{\frac{1}{2}}\right\}^{\frac{1}{2}}$$

$$d_{\sigma y}(z) = 2\sqrt{2}\left\{\left({\sigma_x}^2 + {\sigma_y}^2\right) - \gamma\left[\left({\sigma_x}^2 - {\sigma_y}^2\right)^2 + 4\left({\sigma_{xy}}^2\right)^2\right]^{\frac{1}{2}}\right\}^{\frac{1}{2}} \tag{3.4}$$

$$\gamma = \operatorname{sgn}\left({\sigma_x}^2 - {\sigma_y}^2\right) = \frac{{\sigma_x}^2 - {\sigma_y}^2}{\left|\,{\sigma_x}^2 - {\sigma_y}^2\,\right|}$$

If ${\sigma_x}^2 = {\sigma_y}^2$ then these adjusted equations are used.

$$d_{\sigma x}(z) = 2\sqrt{2}\left({\sigma_x}^2 + {\sigma_y}^2 + 2\left|\,{\sigma_{xy}}^2\,\right|\right)^{1/2}$$

$$d_{\sigma x}(z) = 2\sqrt{2}\left({\sigma_x}^2 + {\sigma_y}^2 - 2\left|\,{\sigma_{xy}}^2\,\right|\right)^{1/2}$$

3.1.1.2 Beam Quality Factor (M^2)

The beam quality factor, or M^{2*} as it is more commonly referred to, is a value which describes how quickly a beam diverges as compared to an idealized Gaussian beam of the same wavelength λ. A more complete definition from the ISO standard is: "...ratio(s) of the beam parameter product along the principal axes of the beam of interest to the beam parameter product of a diffraction-limited, perfect Gaussian beam of the same wavelength λ" [32]. In other words, a perfectly Gaussian beam has an M^2 value of one. The definition of the beam parameter product will be covered later in Sec. 3.1.1.5.

M^2 can be used to derive other beam characteristics or predict how the beam diameter changes as it propagates through space. [32]

In the beam characterization software, M^2 is found by fitting the set of diameters calculated from the planar intensity data. First, a second order polynomial fit is applied to the set of diameters to get rough estimates of the beam characteristics. See Eqs. (3.5-3.10) for how these values are calculated.

$$d_\sigma(z) = \sqrt{a + bz + cz^2} \tag{3.5}$$

$$z_0 = \frac{-b}{2c} \tag{3.6}$$

*There is no value "M" that is squared. The exponent is purely notational [32].

$$d_{\sigma 0} = \frac{1}{2\sqrt{c}}\sqrt{4ac - b^2} \tag{3.7}$$

$$\Theta_\sigma = \sqrt{c} \tag{3.8}$$

$$z_R = \frac{1}{2c}\sqrt{4ac - b^2} \tag{3.9}$$

$$M^2 = \frac{\pi}{8\lambda}\sqrt{4ac - b^2} \tag{3.10}$$

These values are then used as initial guesses when applying a least squares curve fit to the diameter data. The curve fit is applied to Eq. 3.11 solving for M^2 and $d_{\sigma 0}$ simultaneously with the poly-fit values given as starting points for convergence.

$$d_\sigma(z) = d_{\sigma 0}\left(1 + \left(\frac{4M^2\lambda z}{\pi {d_{\sigma 0}}^2}\right)^2\right)^{\frac{1}{2}} \tag{3.11}$$

Where z is the position along the propagation direction of the beam, and λ is the wavelength of the beam. $z = 0$ at the waist of the beam. Below is a slightly adjusted equation to solve for beam radius instead of diameter

$$\omega(z) = \omega_0\left(1 + \left(\frac{M^2\lambda z}{\pi {\omega_0}^2}\right)^2\right)^{\frac{1}{2}} \tag{3.12}$$

3.1.1.3 Azimuth Angle

The azimuth angle ϕ describes the orientation of the principle axis for a slightly astigmatic beam* relative to the reference frame. Astigmatic beams have a different focus location for each of its principle axes. Since the calculated x and y diameters are always the largest and smallest on a given plane, the principle axis, which is formed by such diameters, is subject to change with each plane as the beam changes shape. The azimuth angle is calculated as follows:

$$\phi(z) = \frac{1}{2}\arctan\left(\frac{2\sigma_{xy}^2}{\sigma_x^2 - \sigma_y^2}\right) \tag{3.13}$$

*General astigmatic beams are covered by the ISO 11146-2 standard and require more complex equations to characterize them. These calculations are not included in the beam characterization software.

If $\sigma_x^2 = \sigma_y^2$ then use the following equations

$$\phi = \text{sgn}(\sigma_{xy}^2)\frac{\pi}{4} \tag{3.14}$$

where

$$\text{sgn}(\sigma_{xy}^2) = \frac{\sigma_{xy}^2}{\left| \sigma_{xy}^2 \right|} \tag{3.15}$$

If the difference between the azimuth angles of any two non-circular profiles is greater than 10° then the beam is considered to be general astigmatic. While general astigmatic beams are beyond the scope of this software it is important to check that the beam being analyzed is simple astigmatic to ensure the calculations performed apply.

3.1.1.4 Divergence Angle

Laser beams are always either increasing or decreasing in diameter*. The rate at which the beam's diameter changes in the far field (see Sec.3.1.1.6 for more information) approaches a linear relationship to the distance from the beam waist. This relationship is captured by either the full angle or half angle divergence, Θ and θ respectively (See Fig. 3.1).

While the divergence angle is truly defined by the limit of the ratio of the diameter to the distance from the waist as follows,

$$\Theta_{\sigma x} = \lim_{(z - z0_x) \to \infty} \frac{d_{\sigma x}(z)}{z - z_{0x}}$$

$$\Theta_{\sigma y} = \lim_{(z - z0_y) \to \infty} \frac{d_{\sigma y}(z)}{z - z_{0y}}$$

it is less computationally expensive to approximate the angle from the M^2 and waist diameters values that was already acquired:

$$\Theta_{\sigma x} = \frac{4M_x^2\lambda}{\pi d_{\sigma x0}}$$

$$\Theta_{\sigma y} = \frac{4M_y^2\lambda}{\pi d_{\sigma y0}}$$

*This is true even in the case of a collimated beam [34]. However, the divergence is minimized.

It was found in this study that the difference between the results of each set of equations is negligible, so the approximation was used.

3.1.1.5 Beam Parameter Product

The beam parameter product, or BPP, is the product of the beam's half-angle of divergence, θ, and its waist radius, ω_0 [35]. The BPP of a beam stays constant regardless of the optical system it propagates through, much like the beam quality factor M^2 [35]. This makes the BPP a great choice as a single value to describe a particular beam.

A perfect Gaussian beam has the lowest possible BPP of $\frac{\lambda}{\pi}$ where λ is the wavelength of the beam [35]. As stated before, M^2 can be described as the ratio of the BPPs of a beam to that of a perfect Gaussian beam at the same wavelength [32].

3.1.1.6 Rayleigh Range

Rayleigh range is the distance that the laser travels before the radius has reached a size that is $\sqrt{2}\omega_0$ where ω_0 is the waist radius [32]. This distance above and below the waist position is often considered the operational range of the laser. However, at ARL Penn State, high-powered lasers such as those used in laser scanning applications are often used outside of this range because the energy intensity is too great. A visual example of the Rayleigh range can be seen in Fig. 3.1 labeled as $\sqrt{2}W_0$. Rayleigh range can be calculated with eq. 3.16.

$$Z_R = \frac{\pi d_{\sigma 0}^2}{4M^2\lambda} \tag{3.16}$$

3.2 Predicting Beam Diameter Throughout Optical Train

A common method used to predict how light propagates through an optical train, or a series of optical components such as mirrors and lenses, is called ray tracing [36]. There is a technique called ray transfer matrix analysis that can be used to compress the many calculations involved in ray tracing into a series of 2x2 matrix multiplications. While ray tracing is incredibly useful in a number of situation, it does not fully capture the intricacies of how laser light propagates through space. Ray tracing assumes parallel rays of light traveling in straight lines, but laser light has a curved wave front due to electromagnetic interactions [37]. Furthermore, a beam's diameter is constantly changing.

These discrepancies are accounted for within the following equations [37].

$$M = \begin{bmatrix} A & B \\ C & D \end{bmatrix} \tag{3.17}$$

$$\omega_{0,\text{out}} = \frac{\omega_{0,\text{in}}}{\left((Cd_{\text{in}} + D)^2 + C^2 Z_R^2\right)^{\frac{1}{2}}} \tag{3.18}$$

$$d_{\text{out}} = -\frac{(Ad_{\text{in}} + B)(Cd_{\text{in}} + D) + ACZ_R^2}{(Cd_{\text{in}} + D)^2 + C^2 Z_R^2} \tag{3.19}$$

Where M is the combined optical matrix found by multiplying the optical matrix of each individual component in the optical train, $\omega_{0,\text{out}}$ is the output beam's waist radius, $\omega_{0,\text{in}}$ is the input beam's waist radius, Z_R is the Rayleigh range of the beam, d_{out} is the distance the actual waist falls from where the focus would have one believe it would be, and d_{in} is the distance the beam traveled through air to get to the optical system.

A few example of the matrices used for optical components are as follows [36]:

$$\text{Propagation through free space, where d = distance } M = \begin{bmatrix} 1 & d \\ 0 & 1 \end{bmatrix}$$

$$\text{Reflection off a flat mirror } M = \begin{bmatrix} 1 & 0 \\ 0 & 1 \end{bmatrix}$$

$$\text{Through a thin lens, where f is the focal length } M = \begin{bmatrix} 1 & 0 \\ -\frac{1}{f} & 1 \end{bmatrix}$$

3.3 Path Generation Algorithm

AM processes are guided by a series of instructions that control the movement of the printhead, feed rate, laser power, and more. One of the first steps in generating those instructions is to take the computer-aided designed (CAD) file and take digital cross-sections. This process is called slicing [38]. The result is a collection 2-dimensional polylines, also called contour lines, that outline the part to be printed over a series of heights [38]. A path generation algorithm is then used to fill in the space between the

contour lines. While there are many algorithms available*, none could be found that perform in quite the way desired for this investigation. Therefore, a unique, simple algorithm and accompanying software were developed.

3.3.1 Importing Contour Lines

The software used to create CAD files was SolidWorks. The software used to slice the CAD files and generate contour lines was 3DXpert, an add-on for SolidWorks developed by 3D Systems. The sliced data is stored using the Common Layer Interface (CLI) format [40].

3.3.2 Generating Pathing

The LaserMech FiberScan HR™ laser oscillation device used on the AM system in this investigation offers the ability to repeat wave patterns such as circle, sine wave, or triangle wave but does not offer the ability to dynamically adjust this patterned throughout a print. The defining feature that was needed in the new pathing algorithm was the ability to generate a triangle wave pattern with dynamically adjusted amplitude. A MATLAB program was written that could read a CLI file and create polyshape objects for each layer of the part. The polyshape class comes with a multitude of useful functions including intersection detection. The detection of intersections was used to generate the triangle wave path by drawing out a line until an intersection was detected, then changing the direction for a new line to be drawn. This process is repeated until the end of the part is reached.

The process described above takes into account the translational velocity of the printhead and creates waves with a constant period or frequency. With the intersection points and timing data from the translational velocity, a table of instructions can be generated using the Position, Velocity, Time format used by Galil galvanometer controllers.

3.3.2.1 PVT Format

The PVT instruction format is an incredibly useful tool. When in PVT mode, Galil galvanometer controllers can receive instructions that define the position the printhead

*Powder bed fusion (PBF) path planning algorithms often make use of a technique called 'hatching' [39]. Hatching generally makes parallel scan lines while laser scanning often uses triangular, circular, or sinusoidal patterns. A detailed discussion of hatching is outside the scope of this thesis.

needs to move to, the velocity it should have at that point, and the amount of time allotted to get there. These three instructions are needed for each axis of motion being used. The instruction needed to achieve this motion smoothly are generated by Galil's software. In order to maximize user control, very few restrictions are in place while in PVT instruction mode. Therefore, it is of utmost importance to ensure all instructions can be executed safely, without damaging any of the equipment. These checks are built into the path generation software.

In the case of triangle wave patterns, one axis of motion is determined by the desired translational velocity of the printhead. Often this is held constant throughout the deposition of a bead. The other axis of motion contains the oscillation of the triangle wave. Since a full stop was required at each peak the velocity could be specified as zero for each PVT instruction in the axis of laser motion.

The software written for this thesis outputs a plain text file with the PVT data points listed in the format required by the Galil equipment. These files can either be copied directly into print's execution code or be read in from the file during code execution. This allows for physical experiments to be performed in order to verify the predictions found during this thesis. While physical experiments are not included within this thesis, they are the logical next step and will be explored by CIMP-3D in the near future.

3.4 Energy Distribution Simulation Software

When scan amplitude is adjusted dynamically throughout a bead deposition, the energy input to the substrate is not constant. Assuming all other printing parameters are held constant, a decreased scan amplitude would result in a higher energy density due to the same amount of energy would be imparted over a smaller area. As discussed previously, high energy densities can push the process into a highly undesirable and unstable keyholing regime [18]. In order to avoid vaporization, other parameters must be adjusted to compensate for the effects of a variable scan amplitude. By simulating the imparted energy, a rough estimate of how the other parameters must be adjusted is obtained.

The simulation developed is simple in principle. First, a substrate of user-specified size is broken into a mesh of small elements. Then, a Gaussian approximation of the beam's cross-sectional power density distribution is generated using the beam parameters calculated using the beam characterization software. Next, an iterative process using small time steps sums the individual energy distributions along the path. See Fig. 3.4

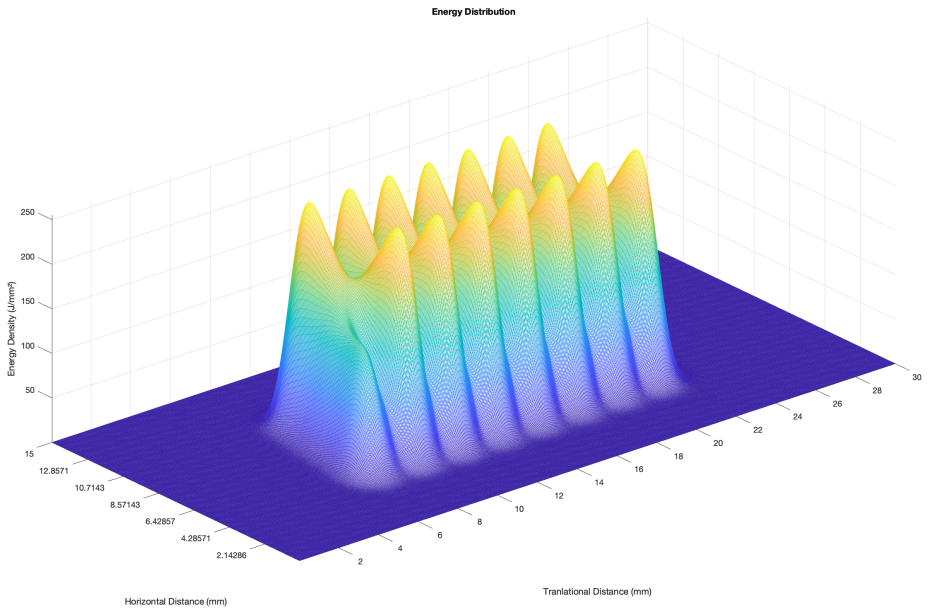

Figure 3.4. An example of the output of the Energy Distribution Simulation software. The power was set to 8kW; scan amplitude was set to 6.3mm; scan frequency was set to 3.5Hz; stand-off distance was set to 402mm; translational velocity was set to 7mm/s.

for an example of what the output looks like.

The result is an approximation of the energy density imparted on the substrate by a laser along an arbitrary path over a defined period of time. It should be noted that this is not a thermodynamic simulation. Heat is not dissipated into the surrounding environment nor the substrate. A simulation such as that is well beyond the scope of this thesis. While the simulation presented does not capture the intricacies of thermodynamics nor laser-material interaction, it does provide a visual guide when searching for regions of concern for vaporization and the effects of changing the processing parameters. While currently not a feature, it is planned to add the ability to take a desire energy distribution as an input and back-calculate the necessary scan pattern and processing parameters require to achieve it.

Chapter 4
Experimental Procedure

Each section in this chapter will discuss the procedure associated with each piece of software utilized, beginning with the beam characterization software.

4.1 Procedure for Beam Characterization

The first step towards simulating the energy imparted by scanned laser beam with varied amplitude is to characterize the laser beam being used. The beam characterization software has all the tools to do this, but first the cross-sectional power density distribution must be measured.

4.1.1 Measuring the Beam

Measurements were taken in the near field[†] of the beam as well as far fields on either side of the focus location. The near field was of utmost interest as it contains the beam's waist, which is crucial for beam characterization. Test runs to confirm the equipment was functioning correctly were conducted using 21 measurement points. For the final data collection, 46 measurements were taken over a range of 100mm with the focus roughly located in the center. A greater concentration of data points were collected in the near field especially when close to the focus location. This was done because the diameter changes most rapidly in the near field. Two additional data sets were taken in the regions past that captured in the first measurement.

The PRIMES FocusMonitor was used to measure the power density distribution. The system was clamped to the down to the processing table with the measurement

[†]The near field is defined by the region of the laser within the Rayleigh range in either direction from the focus. The far field is defined by any region outside the Rayleigh range.

region over the edge. A graphite block submerged in water was placed below to safely absorb the high-power laser light. The robot was positioned so that the waist of the beam would be approximately in the center of the measurement region. Alignment was performed using the low-power 'guide laser' that is attached near the main laser. Then, all personnel retreated to a laser safe control room. For each measurement, the following steps were performed.

1. Turn on the laser.
2. Allow the system to reach a stable temperature*.
3. Start FocusMonitor measurement sequence.
4. Turn off the laser.
5. Check to see if the measurement was well aligned and not saturated.
   (a) Adjust the sensitivity if saturated and repeated whole process.
   (b) Adjust the measurement window if misaligned and repeated whole process.
6. Change position of the printhead for the next measurement.

Once all the data was collected, it was exported as a malleable data format file (.mdf), an ascii-text based file output format used as the input for the beam characterization software. The power density beyond the 100mm range proved to be too low for the FocusMonitor to measure reliably so the data sets were discarded.

4.1.2 Processing the Data

The only step requited to get the results for the near field was to load in the .mdf file in the beam characterization software. Once loaded the values for M^2, beam waist diameter, etc. could be recorded for later use.

4.2 Procedure for Path Generation

A path for the laser to follow was determined by either creating a .cli file from scratch or by slicing a three-dimensional CAD file. In either case, the .cli file was loaded into the Path Generation software along with the parameters describing the properties of the

*Approximately 32°C

triangle wave to be produced. Once generated, a text file was exported that included the PVT data for the path.

4.3 Procedure for Energy Density Simulation

Lastly, the results from the beam characterization analysis as well as select processing parameters were used as inputs in the Energy Distribution Simulation software. The results of three sets of printing parameters are presented in Ch. 5. The parameters that were held constant are provided in Tab. 4.1 while those changed between each simulation are provided in Tab. 4.2.

Table 4.1. The parameters that remained constant through each simulation. Laser beam characteristic listed were calculated using the beam characterization software.

Common Parameters	
Substrate Width (mm)	15
Substrate Length (mm)	30
Number of Timesteps	10000
M^2	15.179
Waist Radius (mm)	0.399
Wavelength (nm)	1075
Translational Velocity (mm/s)	7

Table 4.2. The parameters that changed between each simulation.

	Simulation Number		
Property	1	2	3
Laser Power (kW)	10	8	9
Scan Amplitude (mm)	10.1	6.3	5.6
Offset from Focus (mm)	74.6	74.6	114.6
Scan Frequency (Hz)	7.5	3.5	7.5

Chapter 5
Results

This chapter will look at the results produced by the beam characterization software followed by those produced by the path planning software and finally simulation results using three sets of processing parameters. Discussion of the results are in Chp. 6.

5.1 Beam Characterization

The collection the cross-sectional power density distribution for the beam was successful. Fig. 5.1 shows the plots generated from one plane's worth of data. Fig. 5.2(a) contains the plot of the fitted data when the calculated radii are averaged. Fig. 5.2(b) contains the plot of the fitted data while maintaining the difference in radii and the x and y axial directions. Notice that the focus locations in the x and y principle axes are not equal, therefore the beam is considered astigmatic. The azimuth angle does not vary by more than 10° so it is considered simple astigmatic. Therefore the calculations performed by the beam characterization software are valid. Tab. 5.1 gives the numerical values calculated for the beam properties.

Table 5.1. Beam properties calculated from evaluating data for the IGP Photonics ytterbium fiber laser used on the ABB robotic arm system

Property	X	Y	Average
M^2	15.372	14.985	15.179
Waist Position (mm)	40.822	40.114	40.468
Waist Radius (mm)	0.393	0.420	0.406
Rayleigh Range (mm)	29.298	34.375	31.836
Divergence Angle (mrad)	26.798	26.124	26.461
Beam Parameter Product (mm mmrad)	5.260	5.484	5.374

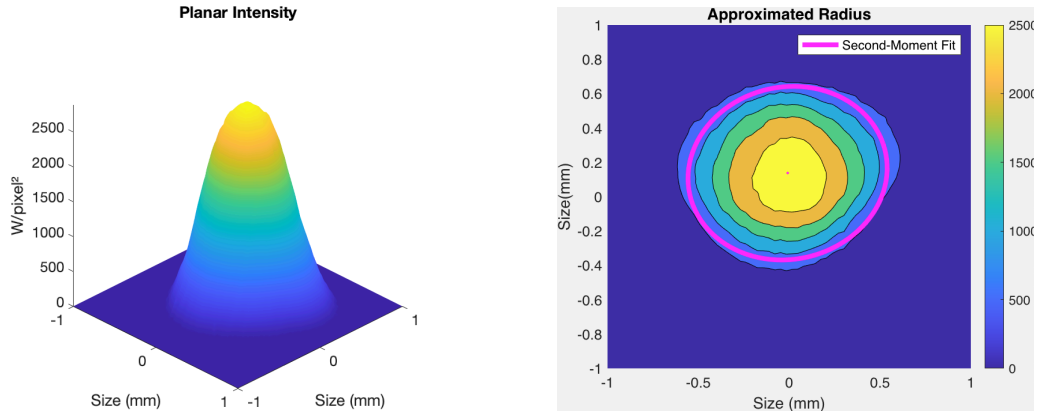

Figure 5.1. A mesh plot and a contour plot generated by the beam characterization software of the cross-sectional power density distribution of the laser 30.468mm past focus. 5.1(b) also includes the calculated beam shape as well as the center point, shown in pink.

Fig. 5.3 shows a plot of the beam's diameter as it propagates through the optical system, starting when it exits the optical fiber. Calculations using Eqs. 3.17 - 3.19 were performed using the input waist diameter as the diameter of the optical fiber. The predicted values for the waist diameter and waist location were within 1% of the measured values.

5.2 Path Planning

Paths were generated using a .cli files that denoted beads with a 7.5mm region of constant scan width followed by a 7.5mm region of attenuating amplitude. The maximum scan width varied for each simulation, but the minimum scan width was set to 1mm for each. See Fig. 5.4 for plots showing the scan paths.

5.3 Energy Distribution

Fig. 5.5 shows the isometric views of simulations run using parameters listed in Tab. 4.1 and Tab. 4.2.

Power density distributions approximations for half a scan period were also generated using the same parameters found in Tab. 4.1 and Tab. 4.2. The resultant plots can be seen in Appendix-D. They were created by super-imposing one thousand Gaussian power density distributions along the scan width. This is a good approximation assuming that the scan velocity of the beam is at least an order of magnitude larger than the

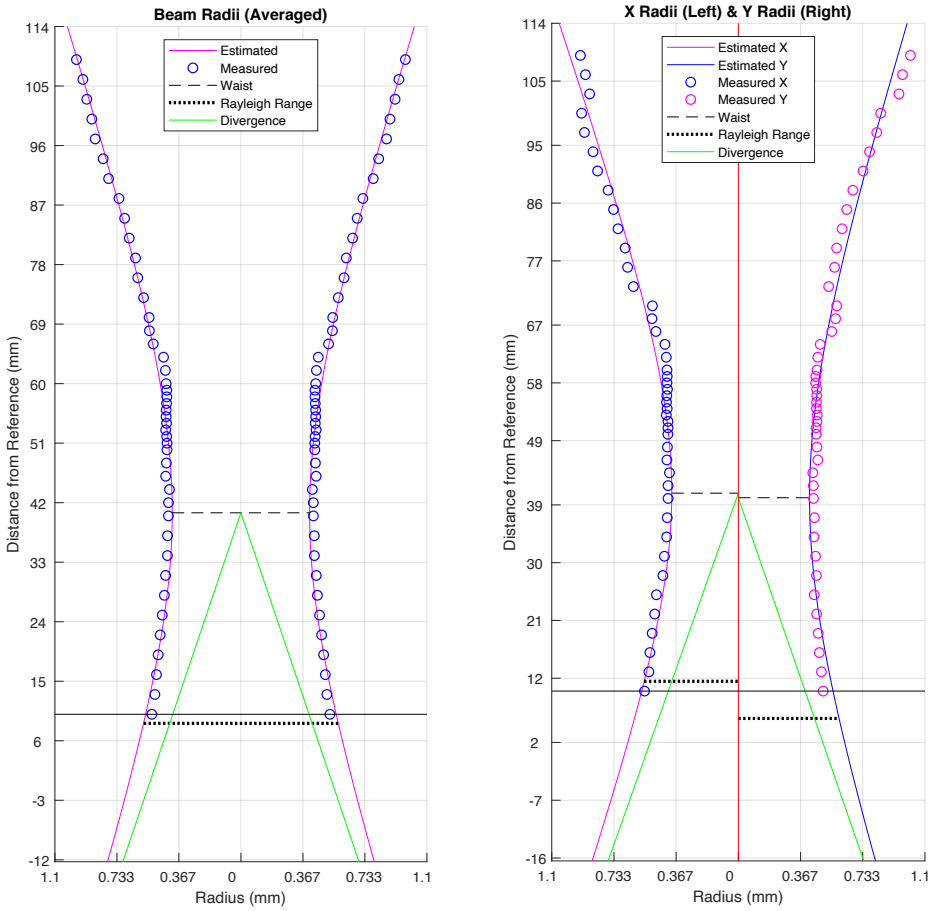

(a) Plot of the average beam radii.

(b) Plot of the X and Y radii side-by-side.

Figure 5.2. Plots of the beam radii produced by the beam characterization software using the cross-sectional power density distribution data from the near field measurements of the IPG ytterbium continuous wave fiber laser through ARL Penn State's large format additive system optics.

translational velocity of the print head. The resulting distributions can be used a heat source input in an FEM thermal analysis software. The input power could be improved upon by using the Goldak [41] double-ellipsoidal model instead of Gaussian distributions. For more information regarding the Goldak method, please refer to Sec. 8.3.

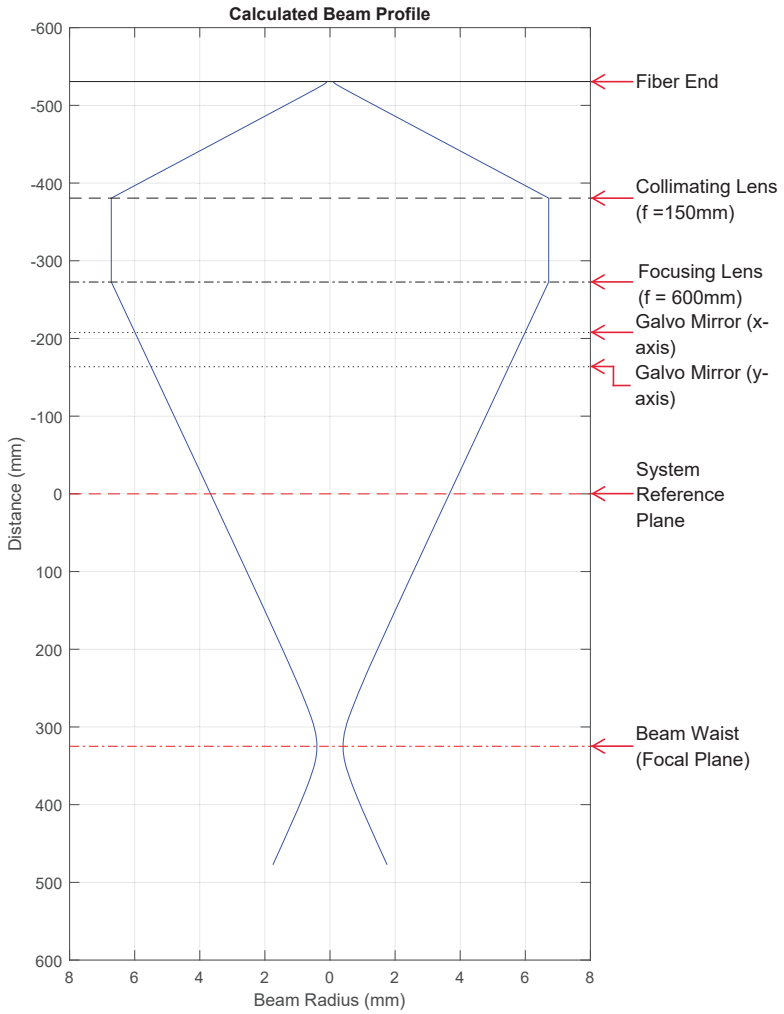

Figure 5.3. Plot of the beam diameter throughout its entire path beginning from the end of the optical fiber. Important locations are denoted with red lines and optical components are denoted with black lines.

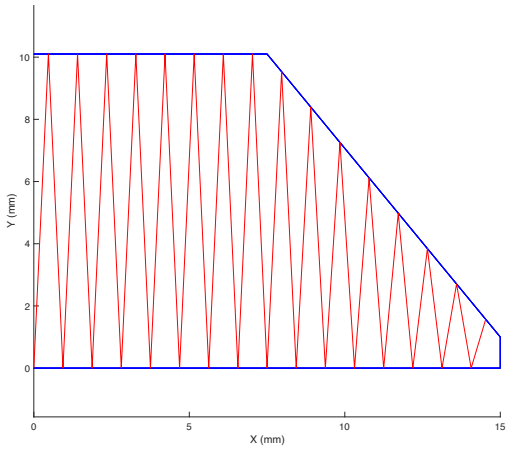

(a) Scan path of max amplitude 10.1mm and frequency of 7.5Hz.

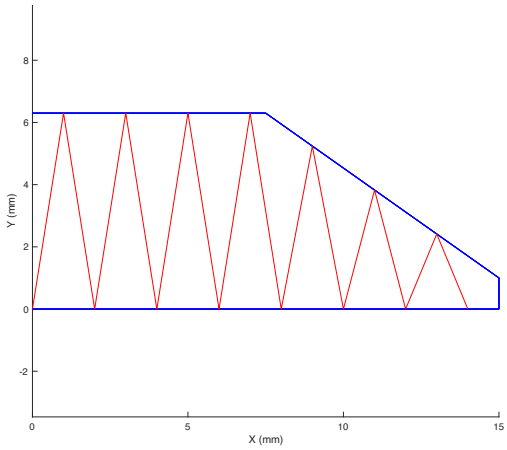

(b) Scan path of max amplitude 6.3mm and frequency of 3.5Hz.

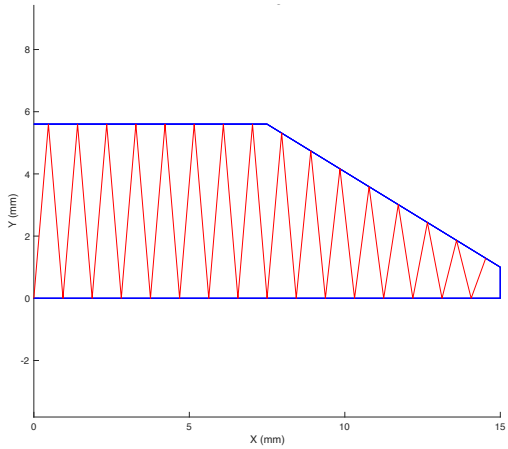

(c) Scan path of max amplitude 5.6mm and frequency of 7.5Hz.

Figure 5.4. Plots of scan paths with a constant amplitude for half their length, followed by a linearly decreasing amplitude to 1mm. Red lines denote the path the laser will take and the blue lines denote the boundaries defined by the .cli file.

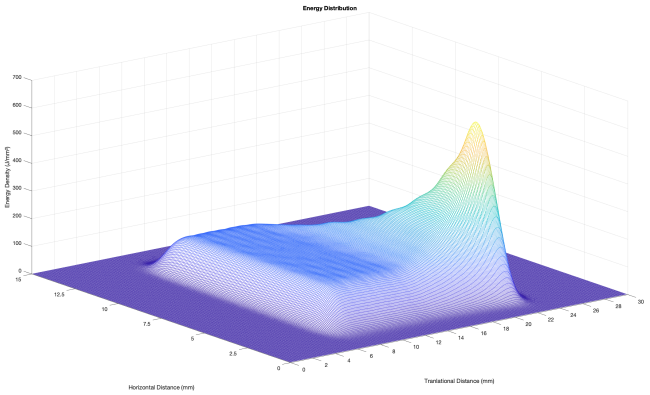

(a) Using parameters for Simulation 1.

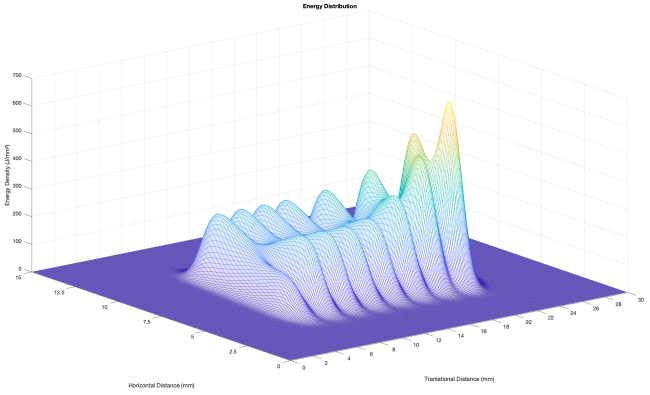

(b) Using parameters for Simulation 2.

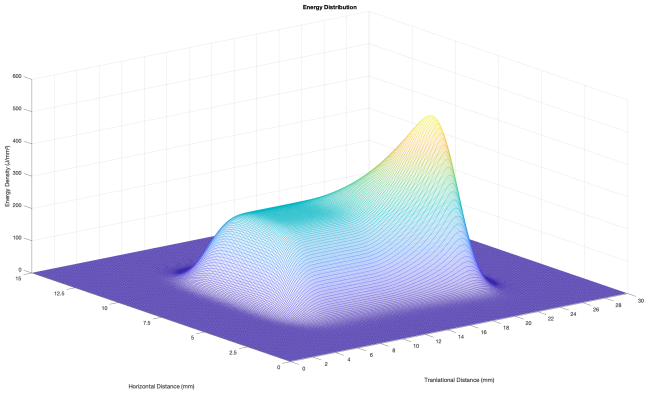

(c) Using parameters for Simulation 3

Figure 5.5. Isometric views of energy simulations. Scan amplitude is held constant for 7.5mm and then attenuates to 1mm over the next 7.5mm. Scaling is equal for the x and y axes, but not the z axis.

Chapter 6
Discussion

6.1 Beam Characterization

The value of M^2 attained through beam characterization seen in Tab. 5.1 falls just outside of the expected range provided by IPG Photonics. Using the provided value for BPP of 4.5mm mrad and accounting for the range in wavelength the expected M^2 value is between 13.090 to 14.680. The calculated, averaged value of 15.179 being just outside the expected value can be explained a few ways. Perhaps the most likely cause is changes to the cross-sectional power density distribution caused by thermal lensing. *De Lange and Otto* [31, 42] saw very similar energy distributions to what was seen in this investigation. Past focus, Fig. 6.1(a), shows a cross-sectional power density distribution that is close to Gaussian. Near focus, Fig. 6.1(d), is closer to a top hat distribution[†]. Before focus, Fig. 6.1(g), has an almost conic distribution. Further before focus, Fig. 6.1(j), perhaps most interestingly exhibits a very non-Gaussian distribution. Most of the power is weighted in the negative y-axial direction. *De Lange and Otto* concluded that the abnormal power distributions can be mostly contributed to thermal lensing onset by particles that have settled on any of the lenses used in manipulating the beam. Any external particles absorb energy from the laser and heat up, creating thermal gradients on the lens [42]. This causes the lens to focus the beam in undesirable ways, like in Fig. 6.1(j). The problem of thermal lensing is worsened by high-power beams as more energy can be absorbed and greater thermal gradients develop. The laser power was set to 10kW during the measurement, which is more than 3 times the power used by *De Lange and Otto*. Fortunately, the substrate is usually located past focus during processing where the power distribution is almost Gaussian. This makes a Gaussian

[†]Top hat distributions have a constant power distribution within a bounded region, outside of which power is zero

distribution a reasonable approximation when simulating the energy input.

Another issue faced with laser characterization was the inability to properly measure certain locations in the optical train. The PRIMES FoucsMonitor, while it does have the ability to adapt to a variety of laser powers, it is not sensitive enough to measure cross-sections with particularly low power densities. It proved impossible to measure the beam more than approximately 70mm away from focus. Additionally, attempts were made to measure the beam in the region it was collimated, but the intensity was too low to get usable data. Despite this, the data gathered closer to focus was sufficient to approximate the radius throughout the optical train with a margin of error under 2%. The results of such calculations can be seen in Fig. 5.3.

6.2 Energy Distribution

While the energy distribution plots in Fig. 5.5 are far from offering a full and complete view of all factors at play when depositing a bead of metal, they do offer information regarding areas that are at risk of excessive vaporization. For example, in Fig. 5.5(a), the region where the amplitude is held constant has an almost constant energy distribution at roughly $130\frac{J}{mm^2}$. The higher frequency of 7Hz reduces the effects of dwell time at the peaks of the triangle scan pattern. Contrarily, Fig. 5.5(b) shows significant increases in energy at the peaks of scan pattern. *Pekkarinen et al.* [18] sought to reduce such increases in energy by dynamically adjusting laser power and increasing scan frequency. Therefore, it is predicted that a more constant energy distribution is more desirable but experiments are needed to confirm this. See Ch. 8 for more information regarding future experimentation.

It is predicted that the geometry of the energy distribution can be used as a way to roughly approximate the resulting cross-sectional geometry of the deposited bead. However, experimentation will be necessary to confirm or deny this prediction.

In all the simulations, a clear increase in energy density develops when the amplitude begins to attenuate. These regions are at an increased risk of vaporization or keyholing. In order to account for this increase in energy other printing parameters would have to be adjusted. One option would be to increase the material feed rate. Since there is more energy in a specific location, it can be used to melt more material. The same amount of energy being used to melt a larger mass of material might possibly keep the melt pool at a temperature below the vaporization temperature. Another option would be to increase the translational speed of the printhead. The linear heat input is effected by the velocity

of the laser spot with respect to the substrate. The velocity vector can be broken into two components. The first being the translational velocity of the printhead and the second being the velocity in the perpendicular direction due to oscillation. Increasing one component of the velocity would increase the magnitude of the velocity vector, reducing linear heat input.

Decreasing laser power is yet another option available. By reducing the input power as the area effected by the laser decreases would be an effective way to avoid excessive heat input. *Pekkarinen et al.* used laser power adjustment to great effect. In their experiments they were able to reduce the effects of excessive heat input at the extremities of the sinusoidal scan pattern by attenuating laser power as a function of distance from the center of the scan pattern. It is possible a similar technique could be used to effect in respect to attenuating amplitudes as well.

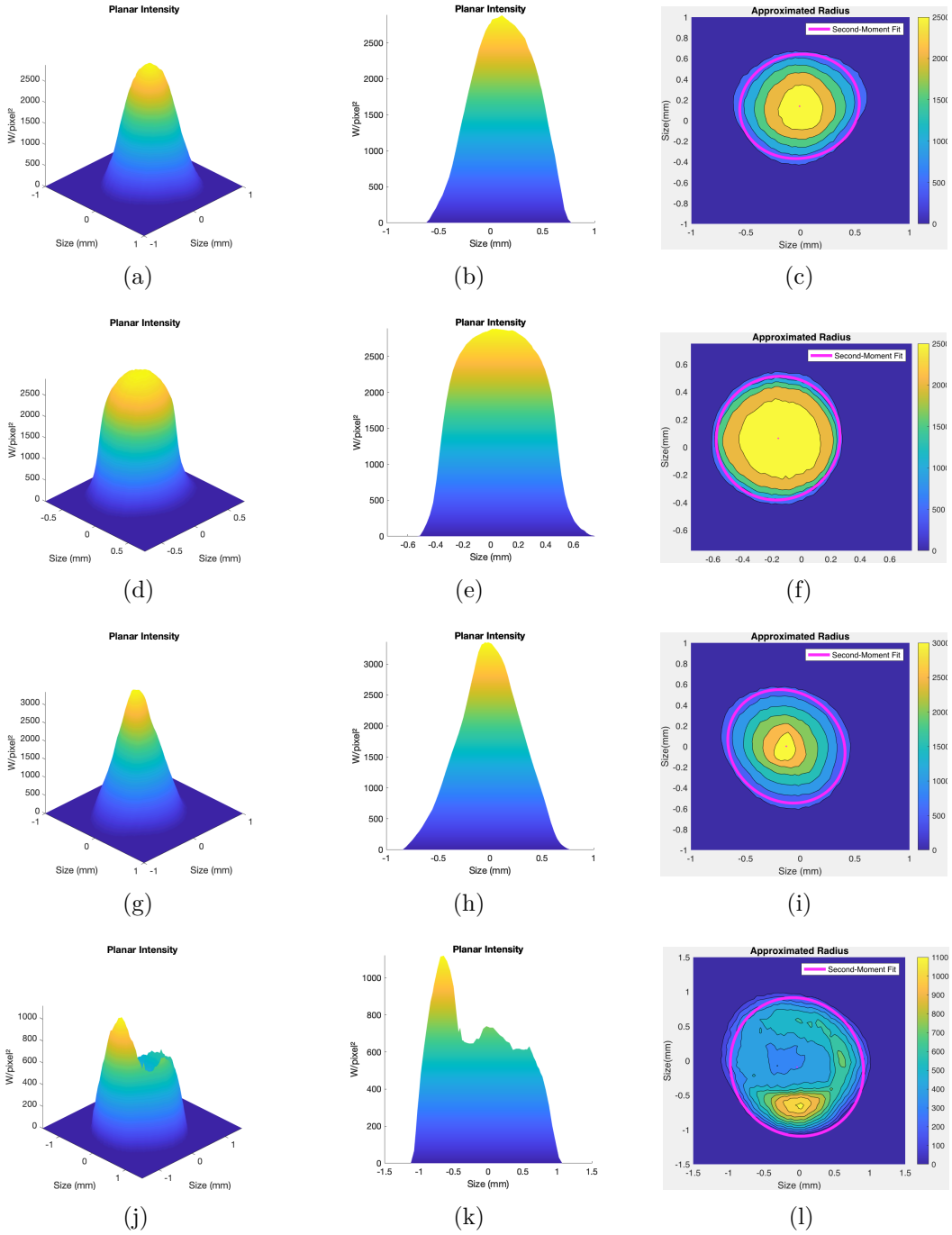

Figure 6.1. Plots of select cross-sections. The locations of the cross-sections by row starting at the top are 30.468mm past focus, 3.468mm past focus, 27.532mm before focus, and 68.532mm before focus

Chapter 7
Summary and Conclusions

In this investigation, an IPG Photonics YLR-12000-C Ytterbium fiber laser was successfully measured and characterized by an independently developed beam characterization software. Regions of varied cross-sectional power density distributions were identified and discrepancies were concluded to be due to thermal lensing. It was concluded that processing past focus is preferable to processing before focus as the power distribution is more stable and can be approximated as Gaussian. The beam diameter throughout the entire optical train was calculated within 2% error from measured values. A reference table, see Tab. C.1, to be used as a guide by operators when adjusting laser spot size was created. PVT pathing instructions were generated that detailed triangular wave patterns which filled contour lines encoded by .cli files. After that, Gaussian cross-sectional power density distributions were generated using the beam characteristics computed earlier. Lastly, the power distributions were used to roughly estimate the energy distribution that would be imparted on the substrate by the laser following the PVT pathing instructions by means of an iterative summation process.

While the generated energy distributions do not offer a complete picture of the deposition process due to the lack of any thermal dynamics, or melt pool fluid dynamics, they do offer a quick way to determine regions at risk of excessive material vaporization. The hope of these simulations is to be used as a guide when adjusting advanced AM strategies to compensate for the increase or decrease in energy density due to an dynamically adjusted scan amplitude. Furthermore, the software developed over the course of this investigation acts as a starting point for future research.

Chapter 8
Future Work

Research into metals additive manufacturing utilizing scanning optics is still a under-explored area of research. Methods involving dynamically adjusting the scan amplitude is particularly open to exploration. The results discussed here in this thesis are merely the beginning of a deeper investigation into the possibilities of variable scan amplitude and the techniques necessary to effectively use it.

8.1 Reducing Bead Overlap

Current AM methods encounter problems when attempting to fill in a region of space that is created by two beads intersecting at an angle. This concept was briefly mentioned in Ch. 1 along with a figure that can been reproduced as Fig. 8.1 for the reader's convenience. Research is currently being done at CIMP-3D with the goal of depositing a steel bead that intersects another bead at an angle of 45° while maintaining a constant bead height. Using current AM techniques, an intersection such as this would either require stopping the deposition before constant with the other bead is achieved or deposit a section of the new bead atop the other[†]. Each option results in a region on the substrate with a lack or, or an excess of deposited material, respectively. Either case is likely to cause issues on subsequent layers because the layer height is no longer constant throughout the cross-section of the part. In order to avoid the issues caused by the beads intersecting at an angle, the scan amplitude will be linearly decreased to compensate for the area of linearly decreasing width.

[†]This region is shown in orange in Fig. 8.1

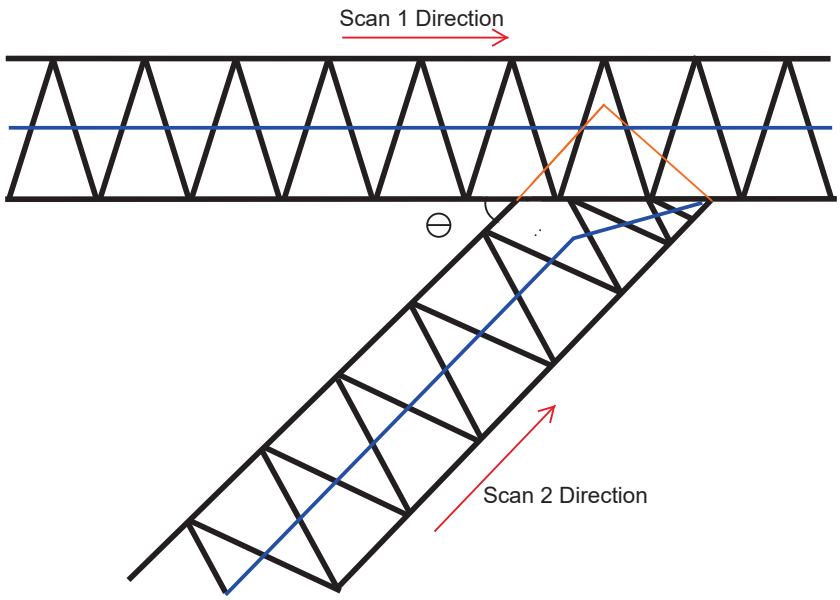

Figure 8.1. This figure, originally shown in Ch. 1, has been reproduced for the reader's convenience. When two scan beads intersect at an angle Θ a region of overlap is created, drawn in orange. This excess of material can lead to issues on subsequent layers. In order to avoid this issue, the width of the bead can be adjusted by reducing the amplitude of the scan pattern of Scan 2. The translational direction of the printhead, shown in blue, is adjusted to remain in the center of the scan pattern to avoid uneven feeding of material.

8.2 Path Planning Algorithm

While the simulations within this thesis only utilized a linearly decreasing scan amplitude there are many applications where the scan amplitude would change in a more complex manner. For example, the path planning algorithm developed for this thesis could be expanded upon to create a beam path regardless of the size of the provided part file.

A range of bead widths could be used to decrease the time to print while maintaining a high print resolution. Regions in which large area must be filled could be filled by beads with a wide scan amplitude, reducing the number of beads necessary. The scan amplitude could be reduced for regions in which small geometries are present. A smaller bead with increases the print resolution by reducing the "stair-step" effect. The "stair-step" effect arises from the inability to perfectly fill a volume with curved edges using only rectangles [21]. The effect is similar to how integrals calculate the volume under a smooth curve using rectangles by making the rectangles' width approach 0. Since the rectangular beads cannot perfectly fit the contour of the part, there are regions where either too

much material is deposited or not enough. Similar to integrals, this effect can be reduced by using a smaller laser spot size or scan width, but doing so comes as the cost of print time. However, with the ability to dynamically adjust bead with by changing the scan amplitude this effect can be negated. Large scan amplitudes can be utilized when the "stair-step" effect is not a concern and smaller amplitudes can be used when necessary.

The current path generation algorithm is not capable of producing instructions for more than one bead. Therefore, when a part that is wider than the FiberScan™ is provided, it cannot successfully output a set of PVT instructions to print it because multiple beads would be required. The author has no knowledge of any path planning algorithms that are able to make use of this; therefore research towards developing such an algorithm is of great interest.

8.3 Goldak Model

A Gaussian distribution is not the most accurate heat source model to represent the input power density distribution for additive manufacturing processes. This is because it only captures the heat being added into the system on the surface of the substrate. Pavelic *et al* [43] developed this method, called the disc model. It is able to model the thermal input better than Rosenthal's [44] application of Fourier's heat flow theory to moving heat sources because it does not assume an infinite heat source. The disc model was further improved by the work of Paley [45] and Wesby [46] who created a model that encompassed the three-dimensional nature of the fusion zone (FZ) to represent the heat source. This leap forward enabled the creation of models that accounted for the penetration of heat into the substrate itself and their results aligned more closely with experimental values. Goldak *et al* [41] then proposed their "double ellipsoidal" that not only captures the penetration of the FZ into the substrate, but also the axial asymmetry of the FZ. The wider leading edge and a trailing "teardrop" shape observed in melt pools could be more accurately represented by two ellipsoids rather than the semi-sphere used Paley and Wesby.

Today the Goldak model is widely accepted as the standard for FEM thermal models. A step forward for the work in this thesis would be to use FEM software that makes use of the Goldak model to more accurately calculate the energy imparted on the substrate.

8.4 Impacts on the Future

Fast, large-scale metals additive manufacturing could have far-reaching implications on both industry and society. The ability to produce a wider variety of parts on demand could lead to a paradigm shift on how industry operates. As discussed previously, parts can be produced on a "as needed" basis rather than being mass produced. Furthermore, generation of metal waste can be drastically reduced by switch to AM methods from subtractive manufacturing methods.

Appendix A
CAD Drawings of Print Head

All images included in this appendix are courtesy of ARL Penn State.

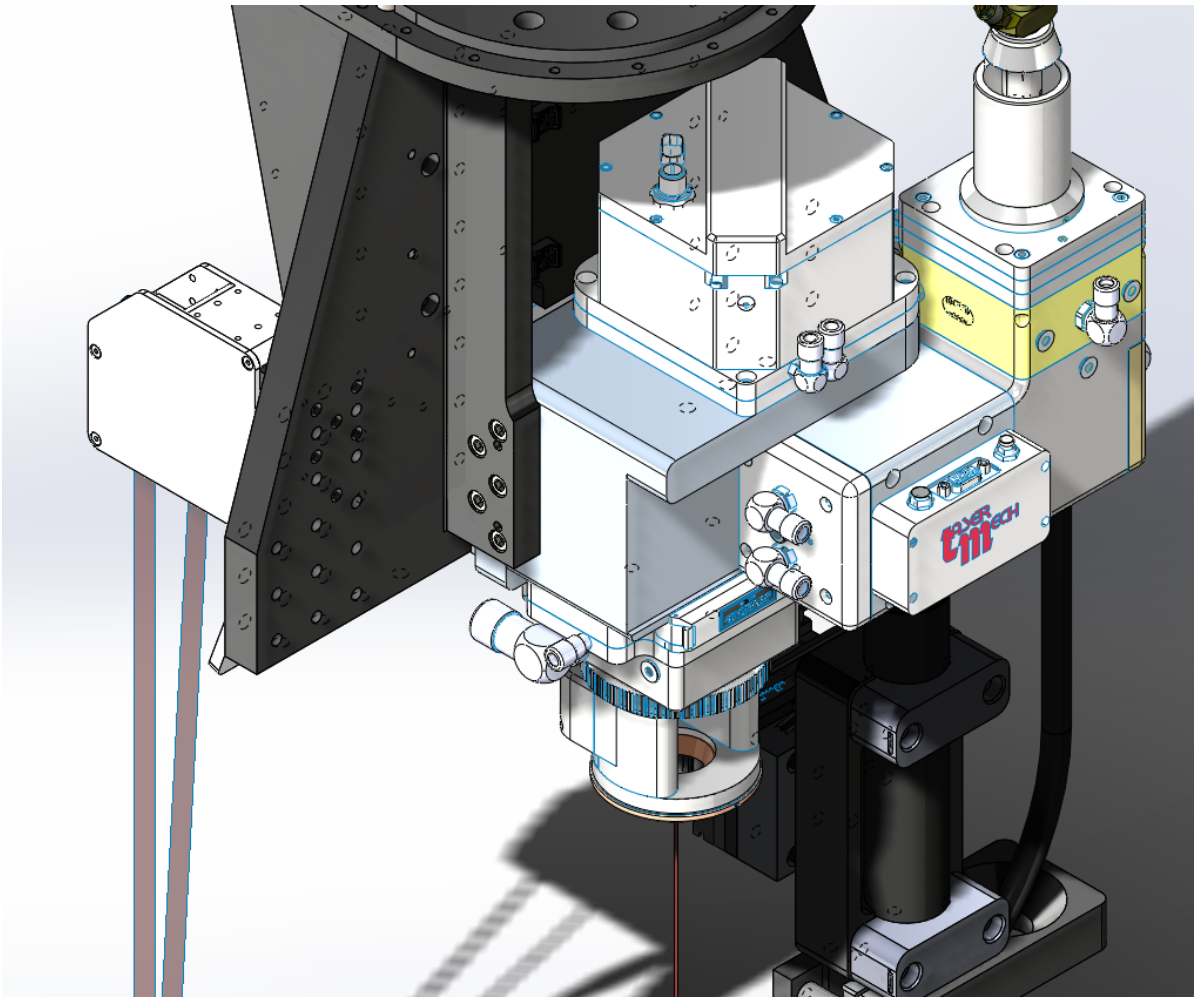

Figure A.1. An isometric view of the printhead of the system used throughout the investigation with a focus on the LaserMech optical control system. Rendered using SolidWorks.

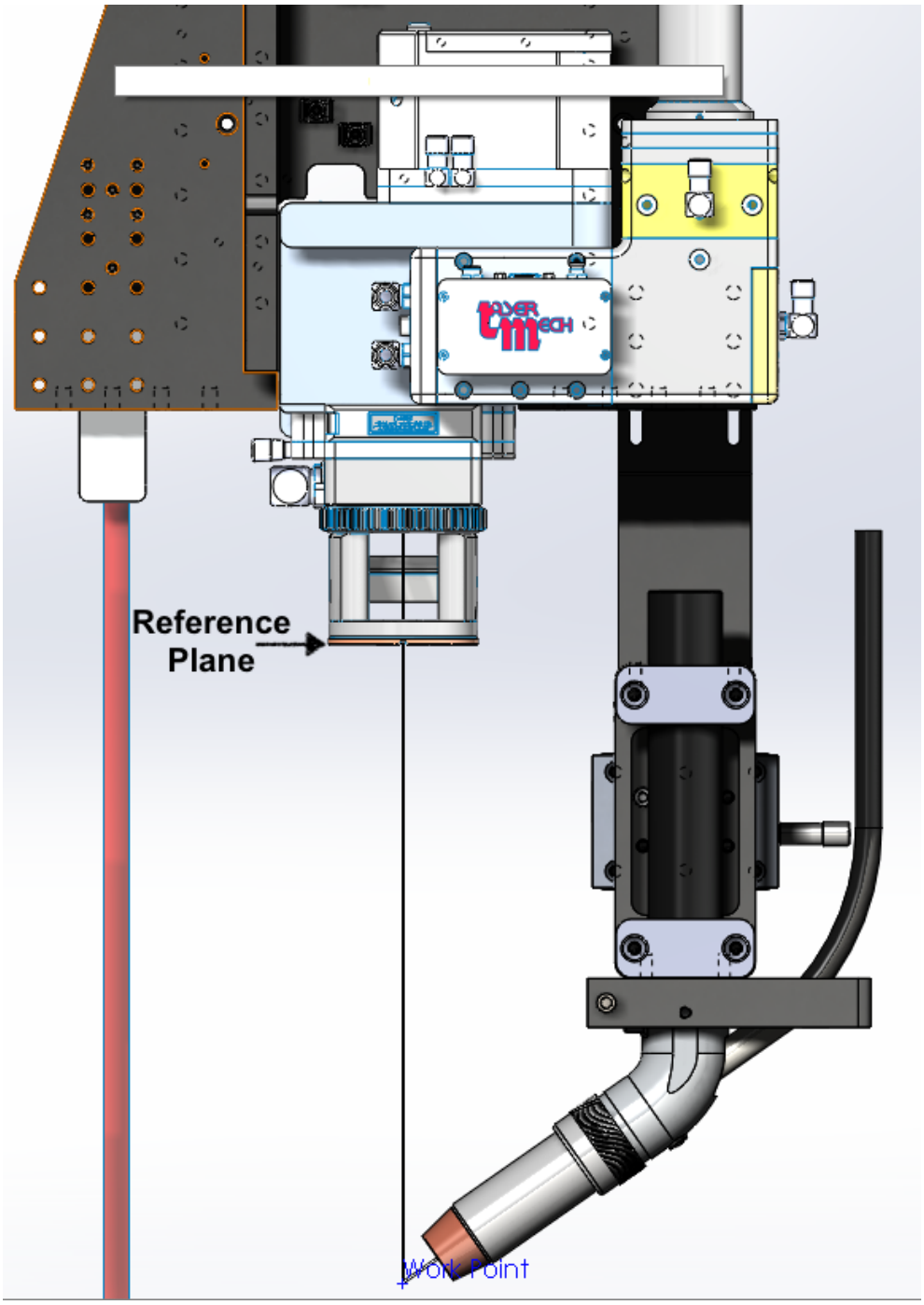

Figure A.2. A frontal view of the printhead of the system used throughout the investigation for this thesis. The laser beam can be seen as a thin black line. Material is fed to the work point at an angle. Rendered using SolidWorks.

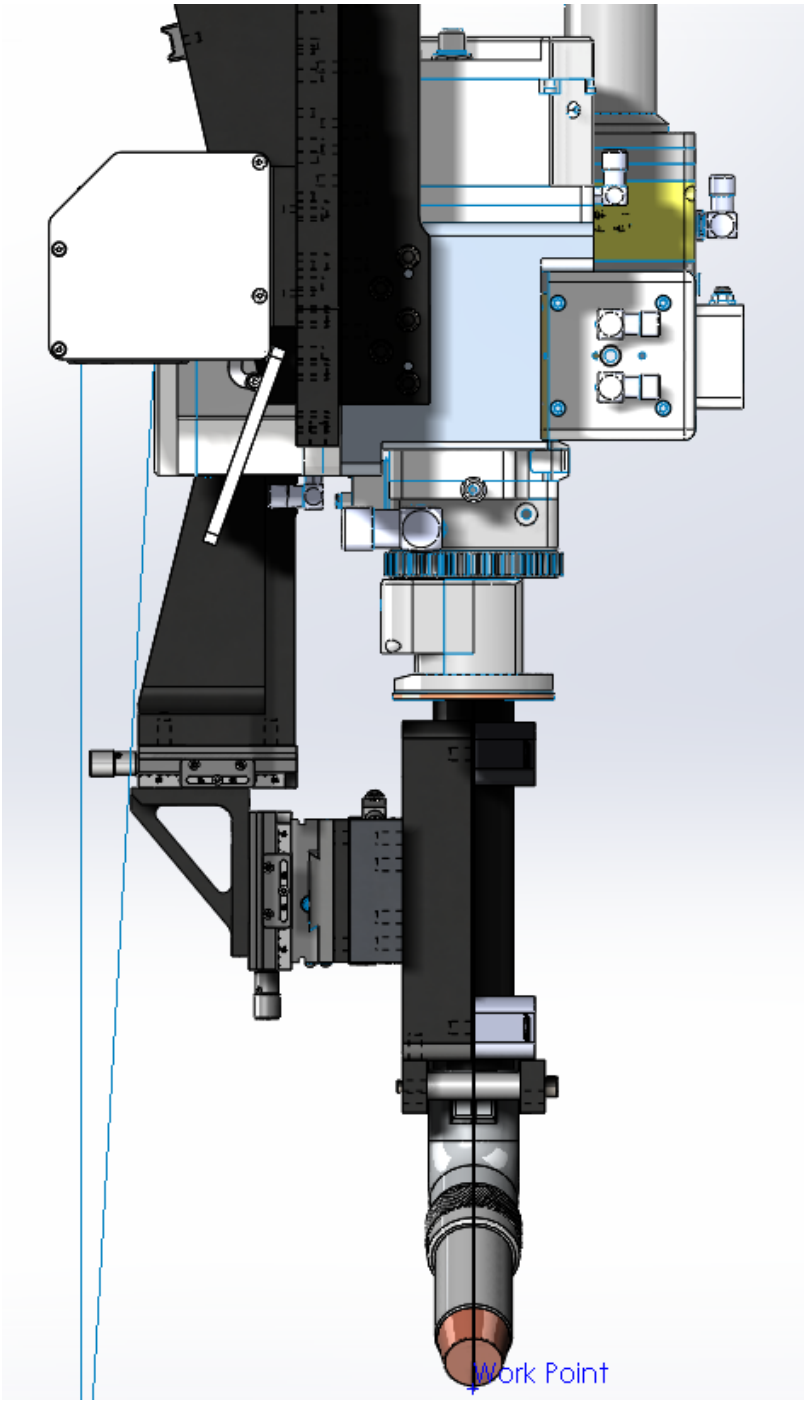

Figure A.3. A side view of the printhead of the system used throughout the investigation for this thesis. Rendered using SolidWorks.

Appendix B
Simulation Results: More Viewing Angles

A variety of different viewing angles are presented here as a way to more easily see the changes in energy density due to both processing parameters as well as attenuating amplitude.

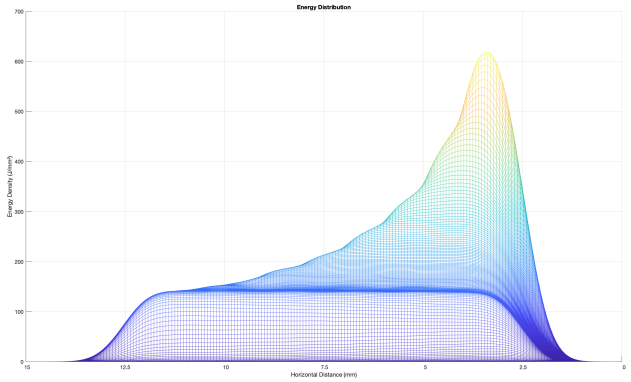

(a) Front view

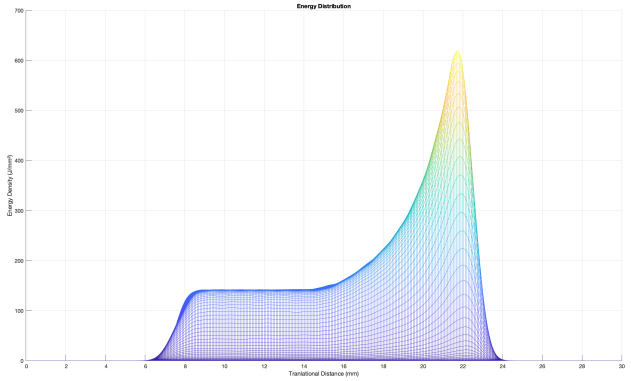

(b) Side view

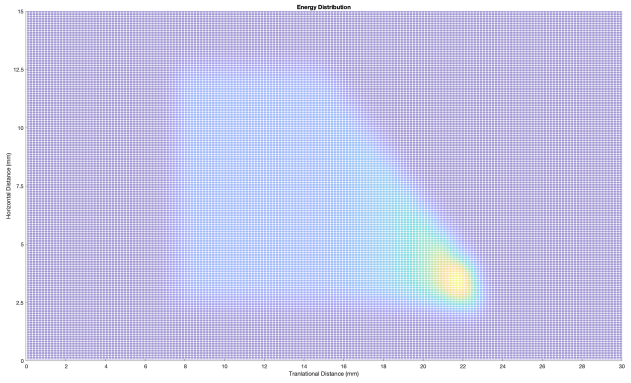

(c) Top view

Figure B.1. Alternate view for simulation 1

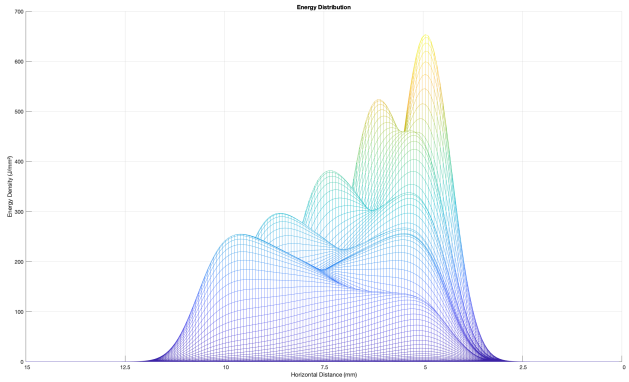

(a) Front view

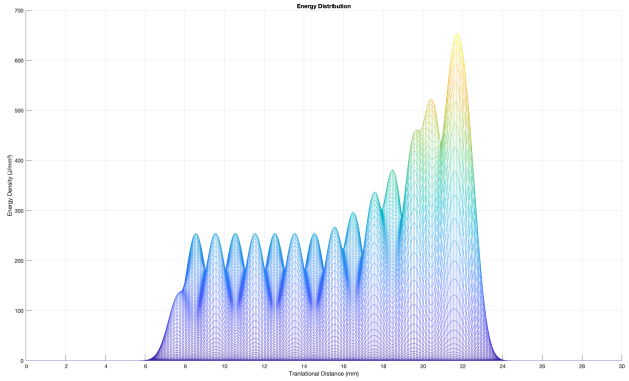

(b) Side view

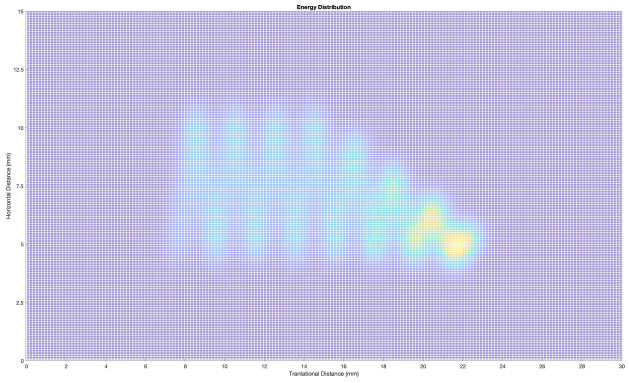

(c) Top view

Figure B.2. Alternate view for simulation 2

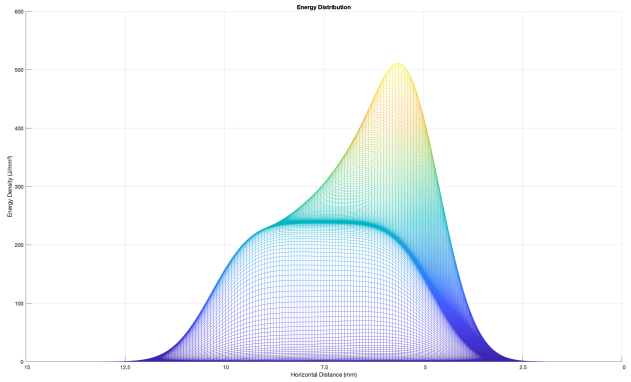

(a) Font view

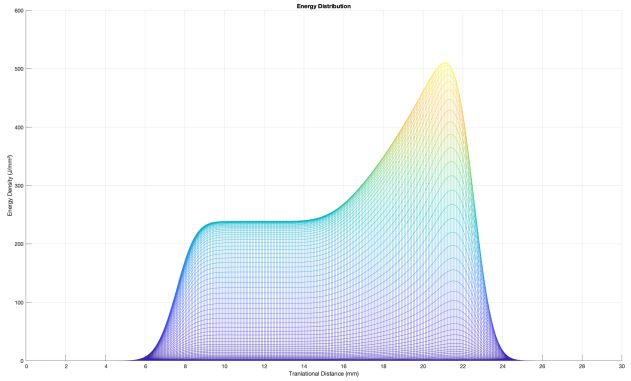

(b) Side view

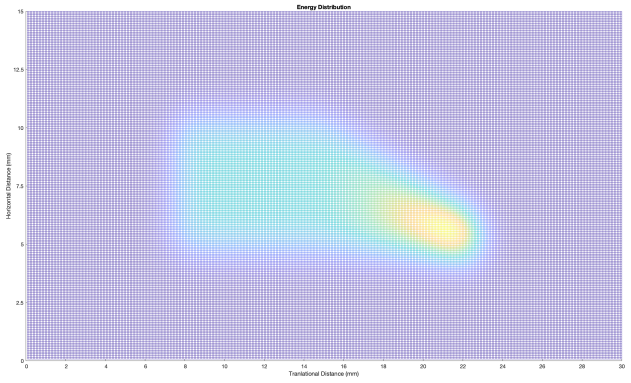

(c) Top view

Figure B.3. Alternate View points for simulation 3

Appendix C
Beam Diameter Reference Table

Table C.1: Pre-tabulated beam radii (in mm) for common off-focus distances for quickly adjusting beam spot size. The reference point is the copper aperture that can be seen in Fig. A.2.

Distance		Beam Radii (All values in mm)		
From Focus	From Reference	Minimum	Average	Maximum
-150	177.4	1.722	1.830	1.947
-145	182.4	1.668	1.772	1.885
-140	187.4	1.614	1.714	1.823
-135	192.4	1.560	1.656	1.761
-130	197.4	1.506	1.598	1.699
-125	202.4	1.452	1.541	1.637
-120	207.4	1.398	1.483	1.576
-115	212.4	1.345	1.426	1.514
-110	217.4	1.292	1.369	1.453
-105	222.4	1.239	1.312	1.392
-100	227.4	1.186	1.255	1.331
-95	232.4	1.134	1.199	1.271
-90	237.4	1.081	1.143	1.211
-85	242.4	1.030	1.087	1.151
-80	247.4	0.978	1.032	1.092
-75	252.4	0.928	0.978	1.033

-70	257.4	0.878	0.924	0.974
-65	262.4	0.828	0.870	0.917
-60	267.4	0.780	0.818	0.860
-55	272.4	0.732	0.766	0.804
-50	277.4	0.686	0.716	0.750
-45	282.4	0.641	0.668	0.697
-40	287.4	0.599	0.621	0.646
-35	292.4	0.558	0.576	0.597
-30	297.4	0.521	0.535	0.551
-25	302.4	0.487	0.497	0.510
-20	307.4	0.457	0.464	0.473
-15	312.4	0.432	0.437	0.442
-10	317.4	0.414	0.416	0.418
-5	322.4	0.402	0.403	0.404
0	327.4	0.399	0.399	0.399
5	332.4	0.402	0.403	0.404
10	337.4	0.414	0.416	0.418
15	342.4	0.432	0.437	0.442
20	347.4	0.457	0.464	0.473
25	352.4	0.487	0.497	0.510
30	357.4	0.521	0.535	0.551
35	362.4	0.558	0.576	0.597
40	367.4	0.599	0.621	0.646
45	372.4	0.641	0.668	0.697
50	377.4	0.686	0.716	0.750
55	382.4	0.732	0.766	0.804
60	387.4	0.780	0.818	0.860
65	392.4	0.828	0.870	0.917
70	397.4	0.878	0.924	0.974
75	402.4	0.928	0.978	1.033
80	407.4	0.978	1.032	1.092
85	412.4	1.030	1.087	1.151
90	417.4	1.081	1.143	1.211
95	422.4	1.134	1.199	1.271
100	427.4	1.186	1.255	1.331

105	432.4	1.239	1.312	1.392
110	437.4	1.292	1.369	1.453
115	442.4	1.345	1.426	1.514
120	447.4	1.398	1.483	1.576
125	452.4	1.452	1.541	1.637
130	457.4	1.506	1.598	1.699
135	462.4	1.560	1.656	1.761
140	467.4	1.614	1.714	1.823
145	472.4	1.668	1.772	1.885
150	477.4	1.722	1.830	1.947

Appendix D
Power Density Distribution Plots

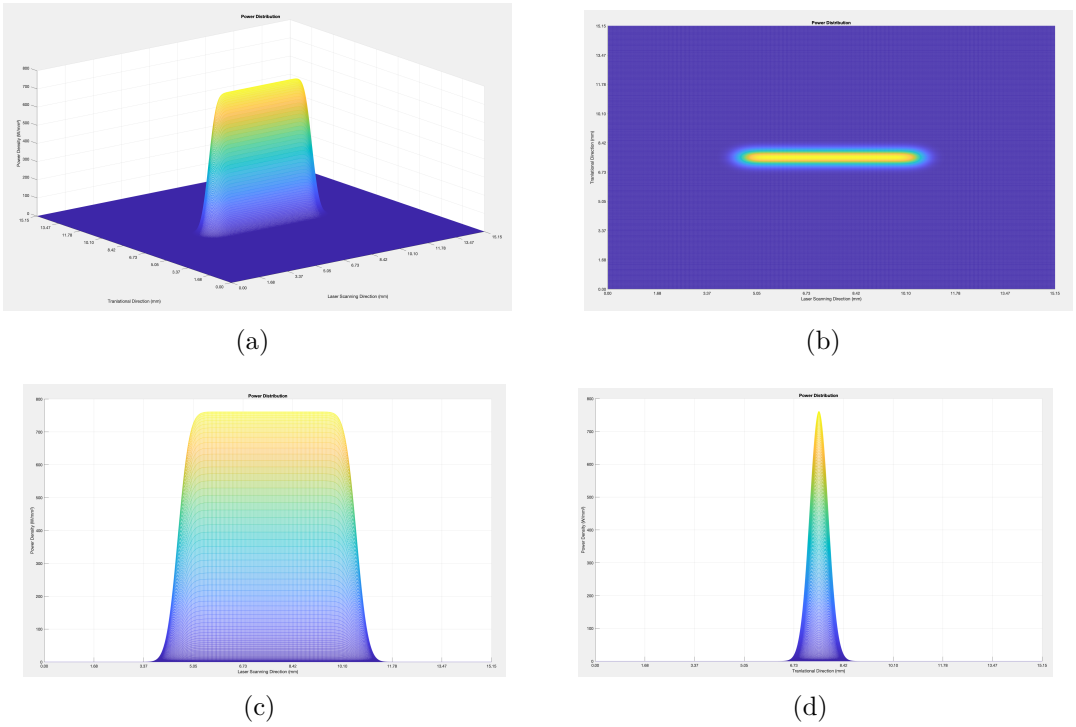

(a) (b)

(c) (d)

Figure D.1. Plots of numerically integrated power density distributions. All calculations where performed using one hundred super-positioned Gaussian beam power density distributions with a workspace resolution of one million points. Scan parameters follow those used in the energy density calculations for scan 1.

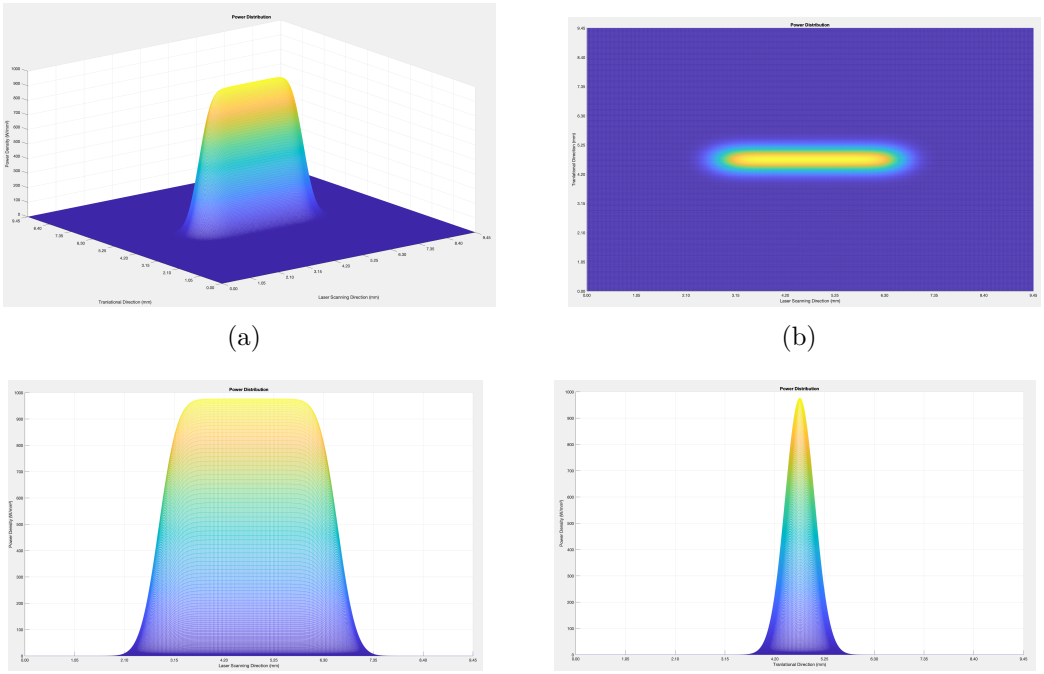

(a) (b)

(c) (d)

Figure D.2. Plots of numerically integrated power density distributions. All calculations where performed using one hundred super-positioned Gaussian beam power density distributions with a workspace resolution of one million points. Scan parameters follow those used in the energy density calculations for scan 2.

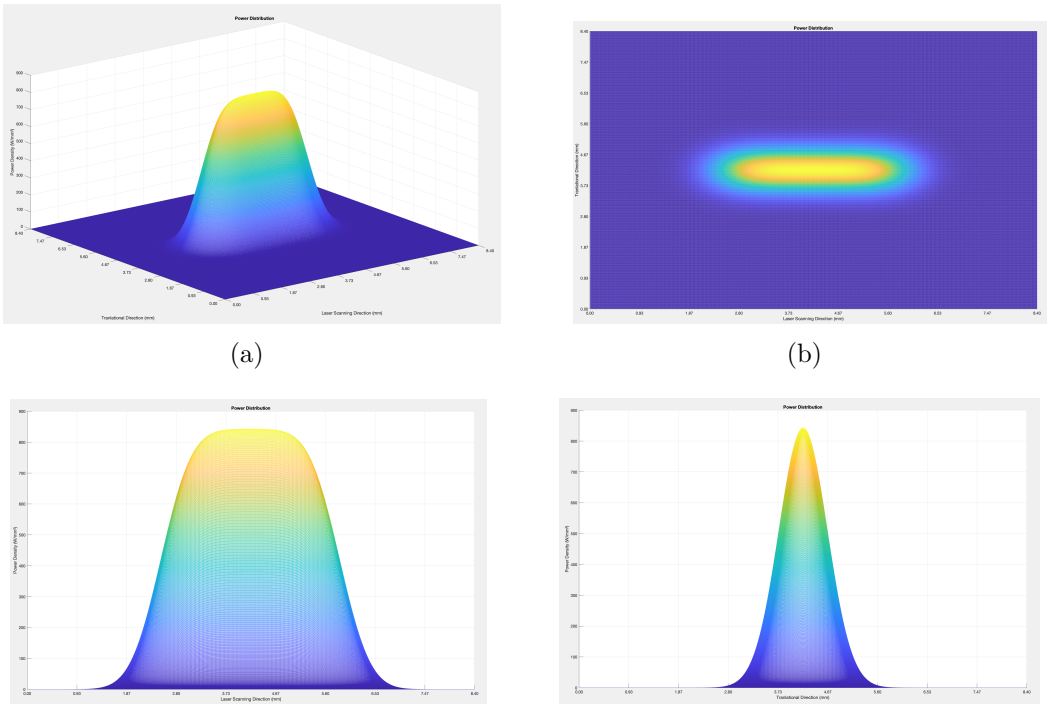

(a) (b)

(c) (d)

Figure D.3. Plots of numerically integrated power density distributions. All calculations where performed using one hundred super-positioned Gaussian beam power density distributions with a workspace resolution of one million points. Scan parameters follow those used in the energy density calculations for scan 3.

Appendix E
Non-technical Abstract

Laser beams are one of the preferred methods of delivering energy for additive manufacturing (AM) systems. They concentrate a very large amount of energy over a small area which is ideal for melting material. However, traditional linear translation of the laser greatly reduces the maximum power that can be imparted during an AM process. If too much energy is concentrated in a small area of the substrate[†], it can cause vaporization, which is highly undesirable. By introducing a mechanism that can quickly manipulate the laser beam back and forth, such as a galvanometer-based beam scanner[‡], while the printhead moves forward, it allows the laser's energy to be distributed over a larger area. In turn, the energy density at any given unit area is smaller. This allows for higher powered lasers to be employed and more material to be deposited in the same amount of time, making scanning laser optics great for large scale AM builds. The hope of this thesis is to create software tools to expand the understanding of how changing the laser scanning parameters effects the printing process. Specifically, interest in changing the scanning amplitude through the printing process is explored. In order to get predictable and repeatable results from this more complex deposition process, a deeper understanding of the energy distribution must be obtained. First a full image of the laser's energy distribution is obtained through a process called laser beam characterization. Then a scan path utilizing a triangle wave pattern is generated from a 2D slice of a CAD file. Finally, the numerically integrate the energy imparted on the substrate by summing the beam energy over many time steps.

[†]The material upon which new material is being deposited

[‡]Galvanometers detect electrical currents by mechanical effects produced from the current. The motion caused can be used to manipulate mirrors to direct laser beams

Bibliography

[1] Kruth, J.-P., M.-C. Leu, and T. Nakagawa (1998) "Progress in additive manufacturing and rapid prototyping," *CIRP Annals-Manufacturing Technology*, **47**(2), pp. 525–540.

[2] Wohlers, T. and T. Gornet (2014) "History of additive manufacturing," *Wohlers report*, **24**(2014), p. 118.

[3] Schmidt, M., M. Merklein, D. Bourell, D. Dimitrov, T. Hausotte, K. Wegener, L. Overmeyer, F. Vollertsen, and G. N. Levy (2017) "Laser based additive manufacturing in industry and academia," *Cirp Annals*, **66**(2), pp. 561–583.

[4] Wang, Z., T. A. Palmer, and A. M. Beese (2016) "Effect of processing parameters on microstructure and tensile properties of austenitic stainless steel 304L made by directed energy deposition additive manufacturing," *Acta Materialia*, **110**, pp. 226–235.

[5] Ding, D., Z. Pan, D. Cuiuri, and H. Li (2015) "Wire-feed additive manufacturing of metal components: technologies, developments and future interests," *The International Journal of Advanced Manufacturing Technology*, **81**(1-4), pp. 465–481.

[6] Semak, V., J. Hopkins, M. McCay, and T. McCay (1995) "Melt pool dynamics during laser welding," *Journal of Physics D: Applied Physics*, **28**(12), p. 2443.

[7] Ding, D., Z. Pan, D. Cuiuri, H. Li, and N. Larkin (2016) "Adaptive path planning for wire-feed additive manufacturing using medial axis transformation," *Journal of Cleaner Production*, **133**, pp. 942–952.

[8] Klocke, F., C. Brecher, D. Heinen, C.-J. Rosen, and T. Breitbach (2010) "Flexible scanner-based laser surface treatment," *Physics Procedia*, **5**, pp. 467–475.

[9] Barnes, N. P. (2007) "Solid-state lasers from an efficiency perspective," *IEEE Journal of Selected Topics in Quantum Electronics*, **13**(3), pp. 435–447.

[10] Paschotta, R. (2019), "RP Photonics Encyclopedia - Wall-plug Efficiency," . URL `https://www.rp-photonics.com/wall_plug_efficiency.html`

[11] Photonics, I. (2008) *Product Specificiation MODEL YLR-12000*, *Tech. rep.*, IPG Photonics.

[12] Steen, W. M. and J. Mazumder (2010) *Laser material processing*, springer science & business media.

[13] Nycz, A., A. I. Adediran, M. W. Noakes, and L. J. Love (2016) "Large scale metal additive techniques review," in *Proceedings of the 27th Annual International Solid Freeform Fabrication Symposium*, p. 2004.

[14] Williams, R. A., E. Beloni, and E. L. Dreizin (2012) "Ignition of metal powder layers of different thickness by electrostatic discharge," *Journal of Propulsion and Power*, **28**(1), pp. 132–139.

[15] Beuth, J., J. Fox, J. Gockel, C. Montgomery, R. Yang, H. Qiao, E. Soylemez, P. Reeseewatt, A. Anvari, S. Narra, et al. (2013) "Process mapping for qualification across multiple direct metal additive manufacturing processes," in *Solid freeform fabrication proceedings*, Univ. Tex. Austin, pp. 655–665.

[16] Mukherjee, T., J. Zuback, A. De, and T. DebRoy (2016) "Printability of alloys for additive manufacturing," *Scientific reports*, **6**(1), pp. 1–8.

[17] Das, P., R. Chandran, R. Samant, and S. Anand (2015) "Optimum part build orientation in additive manufacturing for minimizing part errors and support structures," *Procedia Manufacturing*, **1**, pp. 343–354.

[18] Pekkarinen, J., A. Salminen, and V. Kujanpää (2014) "Laser cladding with scanning optics: Effect of scanning frequency and laser beam power density on cladding process," *Journal of Laser Applications*, **26**(3), p. 032002.

[19] Takata, A., L. Goldfinch, J. Hinds, L. Kuan, and N. Thomopoulis (1974) *Thermal model of laser-induced eye damage*, *Tech. rep.*, IIT RESEARCH INST CHICAGO IL ENGINEERING DIV.

[20] Pekkarinen, J., V. Kujanpää, and A. Salminen (2012) "Laser cladding with scanning optics: Effect of power adjustment," *Journal of Laser Applications*, **24**(3), p. 7.

[21] Ding, Y., M. Akbari, and R. Kovacevic (2018) "Process planning for laser wire-feed metal additive manufacturing system," *The International Journal of Advanced Manufacturing Technology*, **95**(1-4), pp. 355–365.

[22] Klocke, F., C. Brecher, M. Wegener, D. Heinen, B. Fischer, and D. Do-Khac (2012) "Scanner-based laser cladding," *Physics Procedia*, **39**, pp. 346–353.

[23] Belmondo, A. and M. Castagna (1979) "Wear-resistant coatings by laser processing," *Thin solid films*, **64**(2), pp. 249–256.

[24] Pekkarinen, J. (2015) "Scanning optics enabled possibilities and challenges in laser cladding," *Physics Procedia*, **78**, pp. 285–295.

[25] Pekkarinen, J., A. Salminen, V. Kujanpää, J. Ilonen, L. Lensu, and H. Kälviäinen (2016) "Powder cloud behavior in laser cladding using scanning optics," *J. Laser Appl.*, **28**(3), p. 032007.

[26] Pekkarinen, I., V. Kujanpää, and A. Salminen (2012) "Laser cladding using scanning optics," *Journal of Laser Applications*, **24**(5), p. 9.

[27] Rafatov, I. (2009) "Effect of focusing geometry on the continuous optical discharge properties," *Physics Letters A*, **373**(37), pp. 3336–3341.

[28] Bäuerle, D. (2013) *Laser processing and chemistry*, Springer Science & Business Media.

[29] Semak, V. and A. Matsunawa (1997) "The role of recoil pressure in energy balance during laser materials processing," *Journal of physics D: Applied physics*, **30**(18), p. 2541.

[30] Fathi, A., E. Toyserkani, A. Khajepour, and M. Durali (2006) "Prediction of melt pool depth and dilution in laser powder deposition," *Journal of Physics D: Applied Physics*, **39**(12), p. 2613.

[31] de Lange, D., J. Hofman, and J. Meijer (2005) "Influence of intensity distribution on the meltpool and clad shape for laser cladding," in *Proceedings of the Third International WLT-Conference on Lasers in Manufacturing, Munich*, Citeseer, pp. 1–5.

[32] 11146-1:2005(E), I. (2005) *Laser and laser-related equipment — Test methods for laser beam widths, divergence angles and beam propagation ratios — Part 1: Stigmatic and simple astigmatic beams*, *Standard*, International Organization for Standardization, Geneva, CH.

[33] Bautsch (2015), "Gaussian divergence," .
URL `https://commons.wikimedia.org/wiki/File:Divergenz.Gauss-Strahl.png`

[34] Paschotta, R. (2019), "Collimated Beams," .
URL `https://www.rp-photonics.com/collimated_beams.html`

[35] ——— (2019), "Beam Parameter Product," .
URL `https://www.rp-photonics.com/beam_parameter_product.html`

[36] Gerrard, A. and J. M. Burch (1994) *Introduction to matrix methods in optics*, Courier Corporation.

[37] Goldsmith, P. F., I. M. Theory, and T. Society (1998) *Quasioptical systems: Gaussian beam quasioptical propagation and applications*, IEEE press New York.

[38] Jamieson, R. and H. Hacker (1995) "Direct slicing of CAD models for rapid prototyping," *Rapid Prototyping Journal*.

[39] Foster, B., E. Reutzel, A. Nassar, B. Hall, S. Brown, and C. Dickman (2015) "Optical, layerwise monitoring of powder bed fusion," in *Solid Freeform Fabrication Symposium, Austin, TX, Aug*, pp. 10–12.

[40] Group, C. D. (2019), "COMMON LAYER INTERFACE (CLI)," .
URL `https://www.hmilch.net/downloads/cli_format.html`

[41] Goldak, J., A. Chakravarti, and M. Bibby (1984) "A new finite element model for welding heat sources," *Metallurgical transactions B*, **15**(2), pp. 299–305.

[42] De Lange, D. F., J. T. Hofman, and J. Meijer (2005) "Optical characteristics of Nd: YAG optics and distortions at high power," in *International Congress on Applications of Lasers & Electro-Optics*, vol. 1, Laser Institute of America, p. 1503.

[43] Pavelic, V. (1969) "Experimental and computed temperature histories in gas tungsten arc welding of thin plates," *Welding Journal Research Supplement*, **48**, pp. 296–305.

[44] Rosenthal, D. (1946) "Trans. ASME," .

[45] Paley, Z. and P. Hibbert (1975) "Computation of temperatures in actual weld designs," *Welding journal*, **54**(11), pp. 385s–392s.

[46] Westby, O. (1968) *Temperature Distribution in the Work-piece by Welding*, Technical University of Norway.

Academic Vita

Christopher H. Walsh

EDUCATION

Bachelor of Science, Engineering Science, with honors — Aug. 2016 – May 2020
Master of Science, Engineering Science and Mechanics — Aug. 2019 – May 2021
Schreyer Honors College
Minor: Engineering Mechanics
The Pennsylvania State University, University Park, PA
Concentration: Additive Manufacturing
Studied Abroad in China — Summer 2017

EXPERIENCE

Technical Assistant — May 2015 – Aug. 2018
PRO-MIC Corporation, King of Prussia, PA

- Redesigned two Low-Clearance PRO-MIC systems with CAD software to reduce production costs and delivery time
- Authored an electronic technician procedures manual
- Introduced polymer 3D printing into the office
- Modeled and printed over 50 rapid prototypes and production-level parts
- Performed a cost-benefit analysis of moving the office to a paperless file system

R&D Engineering Intern — Apr. 2019 – Present
CIMP-3D, State College, PA

- Created software that can fully characterize a laser beam and show data graphically
- Designed two parts to be used in additive manufacturing research
- Created software that producing machine pathing data from sliced CAD data
- Collaborated on the design of experiments used to observe the effects of laser scanning on additive manufacturing

TECHNICAL SKILLS

CAD: SolidWorks, Autodesk Inventor, eMachineShop
Programming: MATLAB, Python, LaTeX, C++, HTML, CSS, Java, Verilog
Additive Manufacturing: Flashforge Products, GALIL
Circuitry: Circuit board design, soldering

RECENT PROGRAMMING PROJECTS

Mathematical Modeling and Characterization of Scanner-Based Beam Manipulation for Metals Additive Manufacturing

- Undergraduate thesis topic

Laser Characterization Software

- Calculated beam parameters from planar intensity data

Path Planning Algorithm Using Scanning Pattern

- Generated tool pathing from sliced CAD data for use in additive manufacturing

Mathematical Formulae Functions

- Rewrote MATLAB functions such as Taylor/Fourier Series & Gaussian Elimination

LEADERSHIP/ INVOLVEMENT

Alpha Delta Phi – Nittany Chapter

- Academic Chair — May 2017 – May 2018
- THON Chair — Sep. 2017 – May 2019
- Executive Board member – Treasurer — Dec. 2017 – Dec. 2019
  - Responsible for budgeting and tracking over $130,000 per year